Article

Stage 1: Optimization and Characterization of Protein Nanoparticles for the Targeted and Smart Delivery of Cytochrome c to Non-Small Cell Lung Carcinoma

Vanessa Barcelo-Bovea [1,2], Irivette Dominguez-Martinez [1,2], Freisa Joaquin-Ovalle [1,2], Luis A. Amador [1,2], Elizabeth Castro-Rivera[4], Kristofer Medina-Álvarez[4], Anthony McGoron [3], Kai Griebenow [1] and Yancy Ferrer-Acosta [4,*]

[1] Department of Chemistry, University of Puerto Rico, San Juan, Puerto Rico; liz.diaz2@upr.edu
[2] Molecular Sciences Research Center, San Juan, Puerto Rico; admin.msrc@upr.edu
[3] Department of Biomedical Engineering, Florida International University, Florida, USA; jrieradi@fiu.edu
[4] Department of Neuroscience, Universidad Central del Caribe, Bayamon, Puerto Rico; lissette.arroyo@uccaribe.edu
* Correspondence: yancy.ferrer@uccaribe.edu; Tel.: +1 787-798-3001, Ext. 2164.

Received: date; Accepted: date; Published: dates

Abstract: The delivery of Cytochrome c (Cyt c) to the cytosol stimulates apoptosis in cells were its release from mitochondria and apoptosis induction is inhibited. We developed a drug delivery system consisting of Cyt c nanoparticles decorated with folate-poly(ethylene glycol)-poly(lactic-co-glycolic acid)-thiol (FA-PEG-PLGA-SH) to deliver Cyt c into cancer cells and test their targeting in the Lewis Lung Carcinoma (LLC) mouse model. Cyt c-PLGA-PEG-FA nanoparticles (NPs) of 253 ± 55 and 354 ± 11 nm were obtained by Cyt c nanoprecipitation, followed by surface decoration with the co-polymer SH-PLGA-PEG-FA, and compared to a nanoparticle-free formulation. Overexpression of FA in LLC cells and internalization of Cyt c-PLGA-PEG-FA nanoparticles (NPs) was confirmed by confocal microscopy. Caspase activation assays show NPs retain 88-96% Cyt c activity. The NP formulations were more efficient in decreasing LLC cell viability than the NP-free formulation, with IC_{50}: 49.2 to 70.1 µg/ml versus 129.5 µg/ml, respectively. Our NP system is thrice as selective towards cancerous than normal cells. *In-vivo* studies using tagged nanoparticles show accumulation in mouse LLC tumor 5 min post-injection. In conclusion, our NP delivery system for Cyt c shows superiority over the NP-free formulation and reaches a folic acid-overexpressing tumor in an immune-competent animal model.

Keywords: Cancer; cytochrome c; drug delivery; Lewis Lung Carcinoma; nanoprecipitation.

1. Introduction

Apoptosis evasion is one of the hallmarks in all cancer types [1]. The mitochondrial apoptosis pathway has been extensively studied and is known to be the most commonly hindered apoptotic pathway in cancer cells. Cancer cells can acquire adaptations to avoid cell death such as inhibition of mitochondrial outer membrane permeabilization [2], overexpression of survival-promoting proteins [3,4], caspase inhibition, among others. In recent years the induction of intrinsic or extrinsic apoptotic pathways has been a strategy in the development of new cancer treatments [5]. Cytochrome c (Cyt c) release is one key event of the mitochondrial apoptotic pathway that triggers the caspase activation cascade [6]. It has been shown that deficiency of Cyt c can prevent appropriate apoptosome

formation, inhibiting cell death and promoting cancer [7,8]. Several studies have shown that the direct external delivery of Cyt c to the cell cytosol can activate the caspase cascade and induce apoptosis in a dose-dependent manner [9,10]. Our group and others have developed several drug delivery systems for Cyt c which can induce apoptosis selectively in different cancer types by targeting the mitochondrial apoptotic pathway [11-17]. These systems specifically release the drugs under reducing conditions like the ones found in the cellular cytosol, but not outside the cell, increasing their effective dose and lowering off-targets and premature drug release [18].

One feature that has been used to target cancer cells is their surface overexpression of the folic acid receptor alpha (FR). Folic acid (FA) is involved in DNA biosynthesis and because of their rapid proliferation, changes in cell morphology, and tumor microenvironment, cancer cells have increased demands of FA compared to healthy cells, and thus overexpress the FR. Many cancer therapies have been developed using the FR as a target to enhance cancer detection. This receptor has the advantage of being internalized after interaction with its ligand and it is recycled back to the surface, providing a constant enrichment of the drug target in the extracellular membrane of cancerous cells [19]. Once the FR-targeting drug is internalized, to release drugs selectively within the intracellular (reduced) environment, numerous delivery systems have taken advantage of the difference in glutathione concentration between the internal and external cellular milieu [19].

Protein nanoprecipitation is a structure- and activity-preserving technique that permits the synthesis of Cyt c nanoparticles (NPs) with high induction of caspase activation [17]. Around 80-90% of the caspase activity is retained in Cyt c NPs compared to the native protein (100% activity) in cell-free caspase assays [12,13,16,17]. Taking advantage of these systems and their potential for nanotechnology applications in cancer treatment [20], we developed a drug delivery system for Cyt c. The system consists of Cyt c-based NPs decorated on their surface with the amphiphilic co-polymer folate-poly(ethylene glycol)-poly (lactic-co-glycolic acid)-thiol (FA-PEG-PLGA-SH). The FA moiety of the NPs targets specifically cells overexpressing the FR, and after cellular uptake, the disulfide bond that covalently attaches the co-polymer to the Cyt c NPs is cleaved, Cyt c is released and induces apoptosis [15]. This system offers higher loading capacity in comparison to other nanocarriers because the core of the protein is made 100% of Cyt c, which is the drug itself. Our group has proved in previous studies the selectivity and effectivity of the decorated NPs *in vitro*, in HeLa cells, and *in vivo*, in glioma tumors [12,15]. In this study we demonstrate the superiority of the system when compared to an individual, FA-tagged Cyt c system. We also show the optimization of the NPs synthesis procedure to reduce the NPs diameter and enhance tumor entry when applied systemically. Finally, we tested the improved system *in-vitro* in Lewis Lung Carcinoma (LLC) cells and *in vivo* using a syngeneic (immune-competent) mouse model, which is an effective approach for studying how NP therapies reach their target in the presence of a functional immune system [21].

2. Results

2.1. Folic acid uptake by LLC cells

Cellular uptake of NPs can be compromised by size, hydrophobicity, lack of target of the NP, among other factors [22]. In our system, we addressed this challenge by adding a FA ligand in the surface of the NP to induce FA receptor-mediated endocytosis. To confirm if LLC cells could carry out this process, we studied the FA internalization kinetics by confocal microscopy. To determine FA-mediated uptake, LLC cells were incubated in RPMI medium with no folic acid for a period of 24 h, with either 50 μM of a fluorescently labeled FA construct (FA-PEG-FITC) or a binding specificity control without FA (methoxy-PEG-FITC). Cells were washed and fixed at several time-points (0.5, 1, 2, 4, 6, 12 and 24 h). The fluorescence signal intensity of FITC (488 nm) was quantified (in arbitrary units) per cell and compared between the two constructs. **Figure 1** shows that FA internalization steadily increases for a period of 2 h, where it reaches a plateau. After this time point, the levels of FA detected remained constant, probably due to saturation/recycling of the FR. Incubation with the methoxy-PEG-FITC (mPEG-FITC) control shows no intracellular fluorescence signal. These results support that LLC cells can selectively uptake FA because the fluorescence signal was detected within

Peer-reviewed version available at Cancers 2020, 12, 1215; doi:10.3390/cancers12051215

the cells exposed to FA-PEG-FITC possessing the ligand binding to the FR for subsequent internalization, but not the mPEG-FITC (**Figure 1**). An image of FA-PEG-FITC uptake by LLC cells after a 1 h incubation is shown in **Figure 2**. The LLC cell's cytoskeleton, stained with F-Actin (in red) illustrates the internalization of FA-PEG-FITC (green) and its distribution within the cytosol.

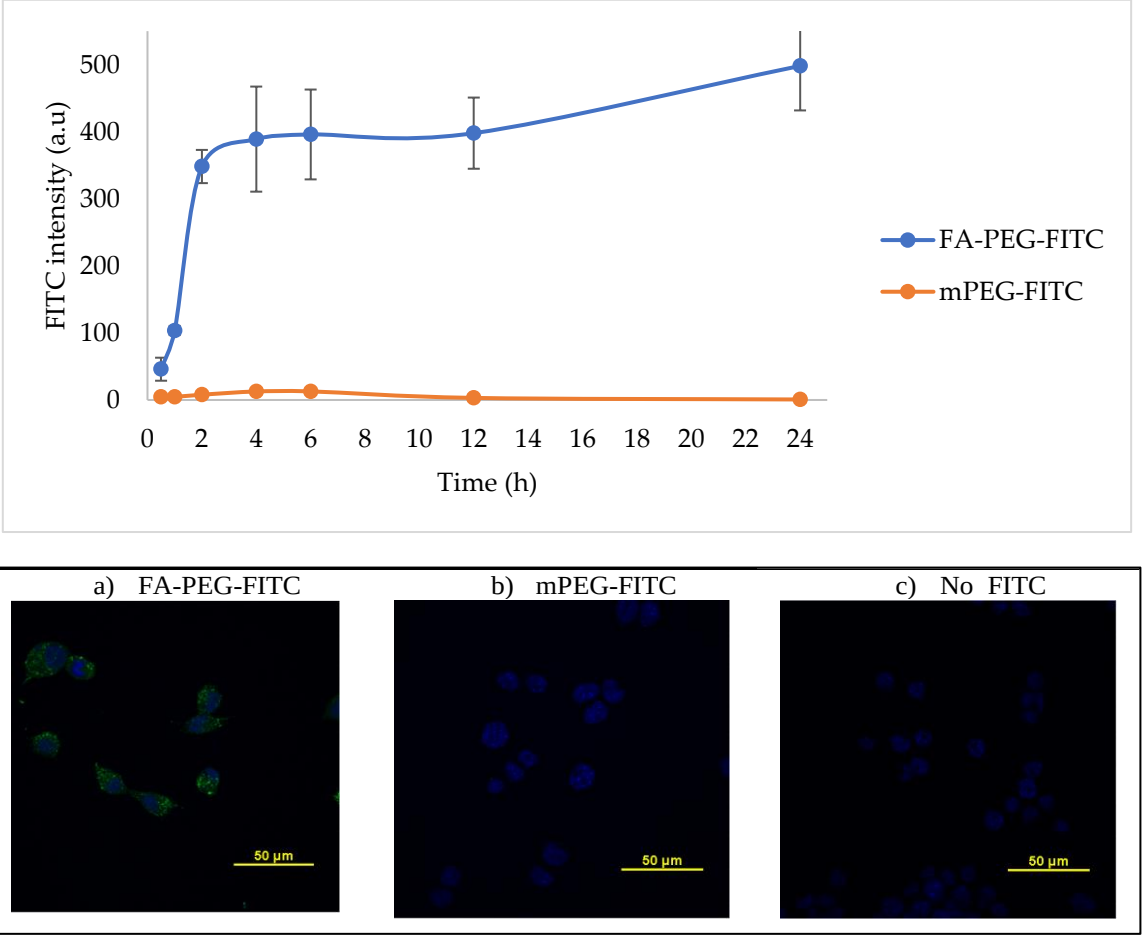

Figure 1. LLC cells uptake folic acid modified with FITC. Upper panel- confocal microscopy was used to measure the intensity of FITC fluorescence signal (Ex. 488nm) in fixed LLC cells incubated with 50µM of FA-PEG-FITC and FITC-PEGm, m=metoxi. Lower panel- representative images of LLC cells illustrate DAPI and FITC channel excitation after 6 h of incubation with: a) FA-PEG-FITC, b) mPEG-FITC, or c) no FITC control. The intensity was calculated using Image J by measuring pixel intensity in each image n=9.

Merged	DAPI (blue)	FA-PEG-FITC (green)	F-actin (red)

Peer-reviewed version available at Cancers 2020, 12, 1215; doi:10.3390/cancers12051215

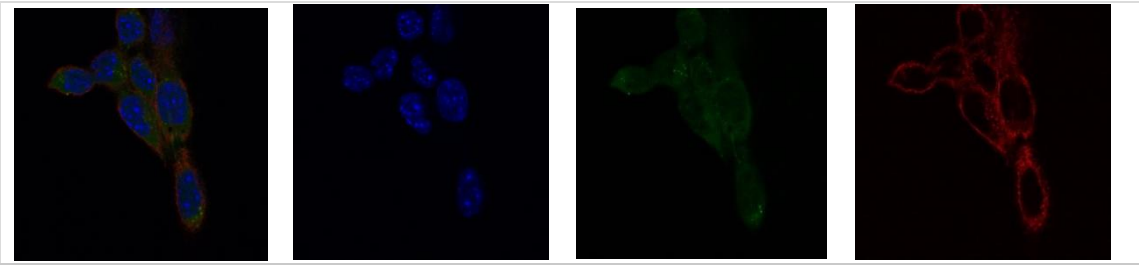

Figure 2. Folic acid distributes in LLC cell's cytosol after uptake. Confocal imaging of LLC cells labeled with cytoskeletal F-actin (red) and nucleus (DAPI) confirm subcellular localization of FA-PEG-FITC (green) throughout the cytosol after 1 h of incubation.

2.2. Synthesis and characterization of a nanoparticle-free Cyt c formulation: Cyt c-PEG-FA

To test the advantage of using a targeted nanocarrier over individual molecules of Cyt c, we constructed a Cyt c-PEG-FA bioconjugate (no NPs). PEG-FA was conjugated to Cyt c lysine groups using the crosslinker succinimidyl-3-(2-pyridyldithio) propionate (SPDP). SPDP is used to conjugate amine-to-sulfhydryls via NHS-ester and pyridyldithiol reactive groups that form cleavable, reducible disulfide bonds with cysteine sulfhydryls. To ensure that there was at least 1 mol of crosslinker per mol of Cyt c, a 1:8 Cyt c: SPDP molar ratio was used in the reaction, which resulted in a final modification of 2 moles of SPDP per mol of Cyt c. Next, the activated Cyt c-SPDP intermediate was reacted with 8 equivalents of PEG-FA resulting in a final modification of 2 moles PEG-FA per each mol of Cyt c (**Table 1**).

To determine the effect of Cyt c modification with PEG-FA on its activity, cell-free caspase 3, 7, and 10 activity assays were made. Our results showed that the final product of individual molecules of Cyt c tagged with FA retained 44 ± 3.4 % of the activity in comparison to native Cyt c (**Figure 3**). This activity loss has already been reported for Cyt c and it is mainly due to a change in the tertiary structure of Cyt c after crosslinking to amine groups, which can lead to its reduction in caspase activation [23].

Table 1. Cytochrome modification with SPDP at different molar ratios of Cyt-c-to-linker [a]

Molar ratio Cyt c to SPDP	Moles of SPDP per mole of Cyt c
1 to 2	0
1 to 4	0.93 ± 0.06
1 to 8	1.95 ± 0.34

[a]Reaction conditions: 2.0 mg/ml Cyt c in PBS-EDTA, pH 7.4 incubated with increasing amounts of SPDP at room temperature for 30 min. The number of reactions prepared for each condition=3.

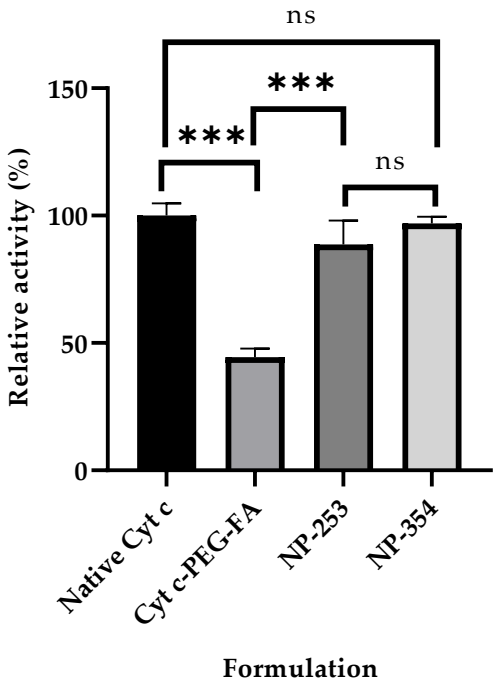

Figure 3. Caspase activity of surface-decorated NPs and NP-free formulation using a cell-free assay. The relative caspase activity for NP-253 and NP-354 surface-decorated NPs was not significantly different between them (ns) or when compared to native Cyt c (ns compared to both NPs). The NP-free formulation Cyt c-PEG-FA, showed significantly decreased caspase activity compared to both NP-253 and NP-354 (***$p < 0.001$, n=3 for each), and native Cyt c (***$p < 0.001$, n=3). Error bars represent the calculated SD.

2.3. Cyt c nanoprecipitation optimization and characterization (synthesis of Cyt c nanoparticles)

A reduction in the NP size has been shown to help significantly the diffusional hindrance and improve the chances for *in vivo* tumor penetration [24]. Aiming to reduce the diameter of the previously reported Cyt c-PLGA-PEG-FA NPs (338 ± 8 nm) [12], four parameters of the nanoprecipitation step were examined: Cyt c solvent, anti-solvent, solvent:anti-solvent ratio, and Cyt c concentration. Four solvents were tested to determine which one was the best to completely dissolve Cyt c and further induce its nanoprecipitation: deionized water, NaCl 10 mM, methyl-ß-cyclodextrine solution, and 10 mM PBS buffer pH 7.4. The best among the tested solvents to induce Cyt c nanoprecipitation was deionized water. Dissolving Cyt c in NaCl 10 mM, methyl-ß-cyclodextrine solution, and 10 mM PBS buffer pH 7.4, induced the formation of aggregates. Also, Dynamic Light Scattering (DLS) measurements were not reliable for the Cyt c NPs obtained using these three last solvents due to aggregate formation. Subsequent nanoprecipitation of Cyt c for NP optimization was performed using deionized water as the solvent.

During the nanoprecipitation step, the dissolved Cyt c in deionized water is mixed with an anti-solvent to obtain an "emulsion" composed of our Cyt c NPs. Thus, we next tested four different anti-solvents (THF, acetonitrile, acetone, and ethanol) to determine if they could differentially affect NP diameter. Acetonitrile had been previously used to generate the Cyt c NPs by our group [12]. The use of tetrahydrofuran (THF) resulted in an increase of the Cyt c NPs diameter compared to the NPs formed using acetonitrile (from 163 ± 13 to 219 ± 9 nm) at a Cyt c concentration of 5 mg/ml. The use of acetone and ethanol did not precipitate Cyt c despite Cyt c being insoluble in these two anti-solvents (**Table 2**). Therefore, our results show that the best anti-solvent to generate Cyt c NPs is (still) acetonitrile.

Using the best solvent and anti-solvent combination according to the above results (water and acetonitrile) we tested the effect of Cyt c starting concentration during nanoprecipitation. NP

diameter and polydispersity index (PDI) were reduced upon lowering Cyt c concentration to from 10 to 5 mg/ml (35% reduction in NP diameter and 51% reduction in PDI) (**Table 3**). There was no statistical difference between the NP diameters obtained using 2.5 and 5 mg/ml Cyt c solutions. When comparing the Cyt c precipitation efficiency or residual caspase activity of NPs obtained from 5 and 10 mg/ml, no statistically significant difference was found using ordinary one-way ANOVA and multiple comparison Tukey's test (95% confidence interval). Caspase 3, 7 and 10 activation by Cyt c NPs remained 88% ± 2 for NP-253 and 96% ± 3 for NP-354, with no significant difference when compared to the native protein, showing an almost intact activity (**Figure 3 and Table 3**).

Table 2. Different anti-solvents used to nanoprecipitate Cyt c [a]

Solvent	Particle diameter (nm)
Acetonitrile	163±13
THF	219±9
Acetone	No Cyt c precipitation
Ethanol	No Cyt c precipitation

[a] Reaction conditions: 5 mg/ml Cyt c in DI water was used. Solvent:anti-solvent ratio of 1:4. The anti-solvents were added a constant rate of 120 ml/h under constant stirring.

After determining that water-acetonitrile was the best solvent and anti-solvent combination, we tested if changing the water-to-acetonitrile ratio affected NP diameter. The addition of higher acetonitrile in the water to acetonitrile ratio 1:4, 1:6, and 1:8 during nanoprecipitation, did not affect the Cyt c NP diameter as shown in **Figure 4**. Our results show that from the four approaches tested, reduction of protein concentration was the only one that helped decrease Cyt c NPs diameter (**Figure 3**).

Table 3. Effect of Cyt c concentration during nanoprecipitation on NP diameter, PDI, precipitation efficiency, and relative caspase 3, 7 and 10 activation of Cyt c NP [a]

Cyt c Concentration (mg/ml)	Diameter (nm)[b]	PDI[b]	Precipitation efficiency (%) [b]	Relative caspase activation (%) [b]
2.5	139 ± 15	0.041 ± 0.03	33.0 ± 7.2	104 ± 10
5	163 ± 13	0.064 ± 0.03	71.9 ± 8.0	96 ± 3
10	251 ± 7	0.13 ± 0.08	84.5 ± 12.3	88 ± 2

[a] Reaction conditions: Nanoprecipitation of Cyt c at different protein concentrations using deionized water as solvent and acetonitrile as anti-solvent. Solvent:anti-solvent ratios used were: 1:8, 1:4, 1:4 for 2.5, 5 and 10 mg/ml Cyt c, respectively. These NP's do not have any surface modification.

[b] Polydispersity index, PDI. Data are the averages and standard deviations of three different batches of NPs.

Peer-reviewed version available at Cancers 2020, 12, 1215; doi:10.3390/cancers12051215

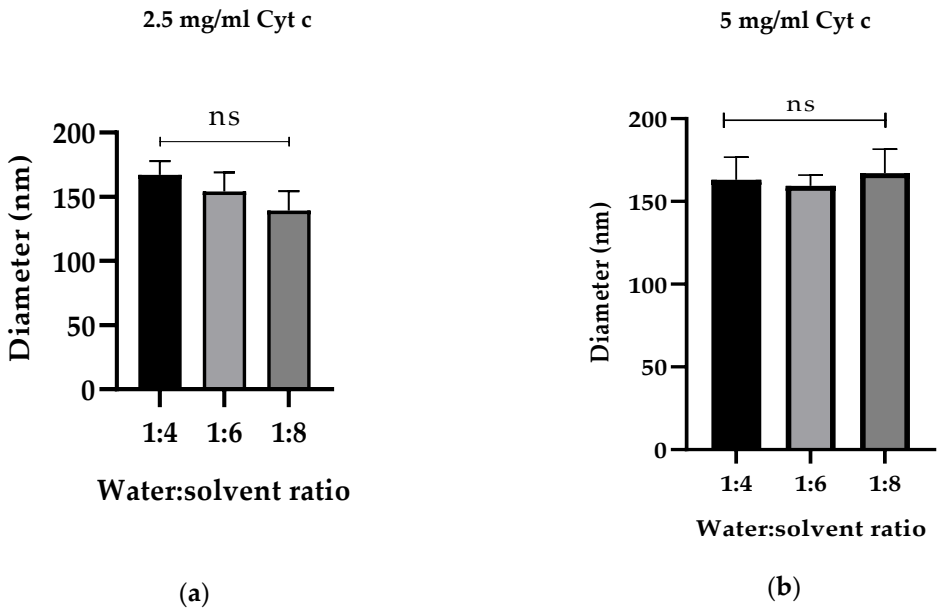

Figure 4. Increased addition of co-solvent during nanoprecipitation does not affect Cyt c NP diameter. Cyt c NPs were obtained adding three different ratios of deionized water-to-acetonitrile (1:4, 1:6, and 1:8) with two different starting Cyt c concentrations: **a)** 2.5 mg/ml, left panel and **b)** 5 mg/ml. One way ANOVA tests were ns among all conditions. Data are the averages of three preparations and the error bars show the SD.

2.4. Cyt c-PLGA-PEG-FA NP optimization and characterization

To optimize Cyt c-PLGA-PEG-FA NPs, several methods to induce a reduction of the Cyt c-PLGA-PEG-FA NP (Cyt c NPs) core size were tested, while maintaining the surface polymer decoration unchanged. The synthesis to add the polymer SH-PLGA-PEG-FA to the NPs was carried out by employing the reaction conditions reported by Morales-Cruz. *et al.* (2014) [17]. To confirm the reproducibility of the synthesis, an ^{1}H NMR of the SH-PLGA-PEG-FA was performed. The ^{1}H NMR spectrum of the copolymer SH-PLGA-PEG-FA confirmed the conjugation of SH-PLGA and COOH-PEG-FA (**Figure 5**). The peaks between 9 and 6 ppm correspond to the aromatic protons in FA, while the peaks between 6 and 1 ppm correspond to both PLGA and PEG, validating the reproducibility of polymer synthesis.

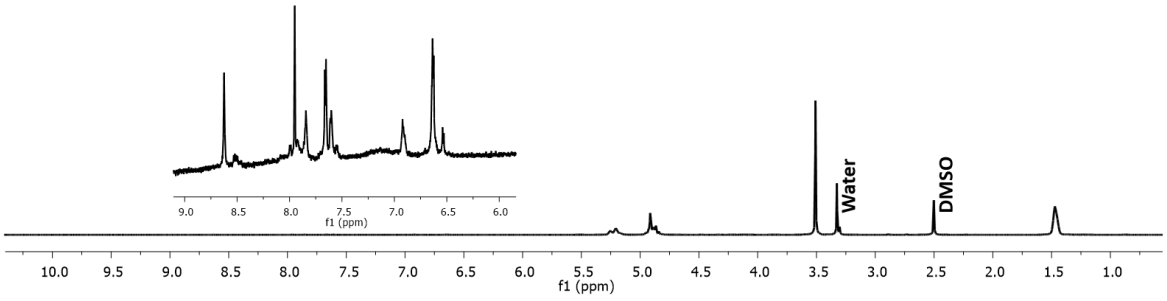

Figure 5. **H^{1} NMR spectrum of the copolymer SH-PLGA-PEG-FA.** The peaks between 9 and 6 ppm correspond to FA protons, while the peaks between 6 and 1 ppm correspond to both PLGA and PEG.

After nanoprecipitation, Cyt c NPs with three different diameters (139, 163, and 251 nm, obtained from Cyt c solutions of 2.5, 5 and 10 mg/ml, respectively) were subjected to surface modification with the crosslinker SPDP, followed by the conjugation of the co-polymer SH-PLGA-PEG-FA. Cyt c NPs alone (without decoration) were found to be stable only in the mix of water:acetonitrile in which they are formed (at least in a 1:4 ratio), but not in aqueous solution alone.

Peer-reviewed version available at Cancers 2020, 12, 1215; doi:10.3390/cancers12051215

The hydrophobic PLGA segment of SH-PLGA-PEG-FA protects Cyt c NPs from dissociating in aqueous solution, while the hydrophilic PEG segment allows Cyt c NPs to solubilize in aqueous solution. However, only Cyt c NPs with diameters of 163 and 251 nm remained stable after being transferred to the aqueous solution, while the 139 nm NPs dissolved (**Table 4**). The smaller the particles, the less surface protection is afforded by the polymer due to increased curvature and thus, it might be necessary to find other strategies to afford smaller NPs for such applications.

Characterization of the Cyt c NPs and Cyt c-PLGA-PEG-FA NPs was made using Dynamic Light Scattering (DLS), zeta-potential, and UV-spectroscopy and Scanning Electron Microscopy (SEM). **Table 4** shows the properties of the Cyt c-PLGA-PEG-FA NPs obtained from undecorated Cyt c NPs with diameters of 163 and 251 nm, that were further modified. After PLGA-PEG-FA conjugation the initial diameter of the Cyt c NP's generated with different Cyt c concentrations increased around 100 nm in both cases. Multiple comparison analysis showed a statistical difference between the diameters of NP-253 and NP-354 ($p < 0.001$). There are no significant differences in encapsulation efficiency, actual loading capacity, and zeta potential between Cyt c-PLGA-PEG-FA NP obtained using 5 mg/ml (NP-253) and 10 mg/ml (NP-354) Cyt c during nanoprecipitation.

To confirm the morphology of the decorated NPs, these were visualized using scanning electron microscopy (SEM) (**Figure 6**). Results show spherical particles with a consistent size distribution for both NP-253 and NP-354, reproducing the ones previously produced by Morales-Cruz *et al*. (2014), but with different sizes.

Table 4. Parameters of Cyt c-PLGA-PEG-FA NPs obtained using 5 mg/ml (NP-253) and 10 mg/ml (NP-354) Cyt c during nanoprecipitation. The same stichometry (molar ratios of Cyt c, crosslinker and SH-PLGA-PEG-FA) was used in both cases. [b]

Nanoparticle name / Parameter	Cyt c NP[a]	NP-253	NP-354
Cyt c used during nanoprecipitation (mg/ml)	2.5	5	10
Diameter before coating with PLGA-PEG-FA (nm)	139±15	163 ± 13	251 ± 7
Diameter after coating with PLGA-PEG-FA (nm)	-	253 ± 55	354 ± 11
PDI	-	0.07 ± 0.06	0.13 ± 0.03
Encapsulation efficiency (%)	0	45 ± 7	48 ± 9
Actual loading (%)	-	62 ± 10	66 ± 10
Relative caspase activity (%)	-	89 ± 9	99 ± 6
Zeta potential (mV)	-	26.9± 5.03	22.4 ± 6.36

[a] The use of 2.5 mg/ml Cyt c during the nanoprecipitation did not yield Cyt c-PLGA-PEG-FA NPs. [b] NP data in the table are the averages of three batches prepared and the respective standard deviations.

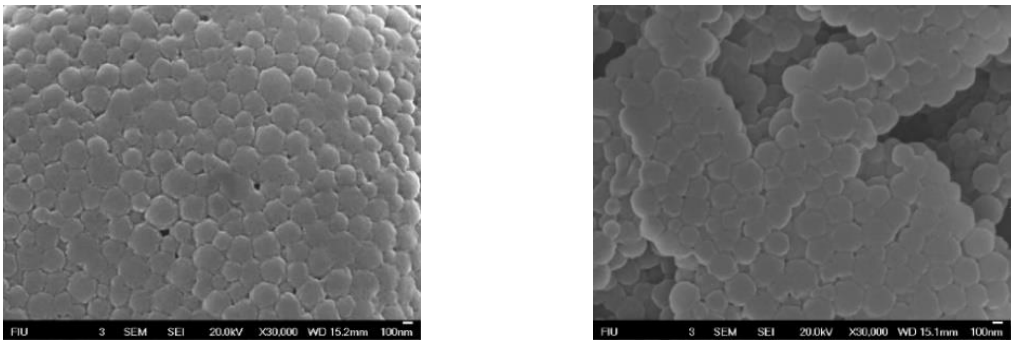

(**a**) (**b**)

Figure 6. Scanning electron micrographs of Cyt c-PLGA-PEG NPs. a) NP-253 and b) NP-354. Scale bar in **a** and **b**:100 nm.

2.5. Release profile of nanoparticles

One of the characteristics that make these NPs a smart targeted drug delivery system is their capacity to respond to stimuli such as changes in pH. The SPDP crosslinker enables NPs to detach their stabilizing PLGA-PEG-FA polymer decoration once they are in contact with a reducing environment, destabilizing the NP and releasing their Cyt-c content. **Figure 7** shows the release profiles of Cyt c-PLGA-PEG-FA NPs (both NP-354 and NP-253) under different reducing conditions, emulating the cell's intracellular (glutathione reducing agent added) or extracellular environment (no glutathione). In both NPs, the optimum release condition was PBS pH 7.4 containing 10 mM glutathione S- transferase (GHS), which simulates the reducing environment inside the cells. Time for 50% release was 1 hr and 2 h for more than a 75% release of the contained Cyt c in the NPs. The release behavior of NP-253 and NP-354 under reducing conditions was not significantly different between them ($p > 0.9$) according to an ordinary one-way ANOVA multiple comparisons analysis. Both NP-253 and NP-354 had significantly lower release under the conditions that simulate the extracellular physiological environment (PBS + 0.001 mM GHS or PBS alone) [25] in comparison to PBS + 10 mM GHS ($p < 0.0001$). The difference between 0 and 0.001 mM GHS was not significant for both of the NP formulations. These results show that due to their stimuli-responsive controlled release, the Cyt c-PLGA-PEG-FA NPs can keep the cargo (Cyt c) encapsulated while they are in an environment like the bloodstream and can deliver it once the system is internalized by cells.

Peer-reviewed version available at Cancers 2020, 12, 1215; doi:10.3390/cancers12051215

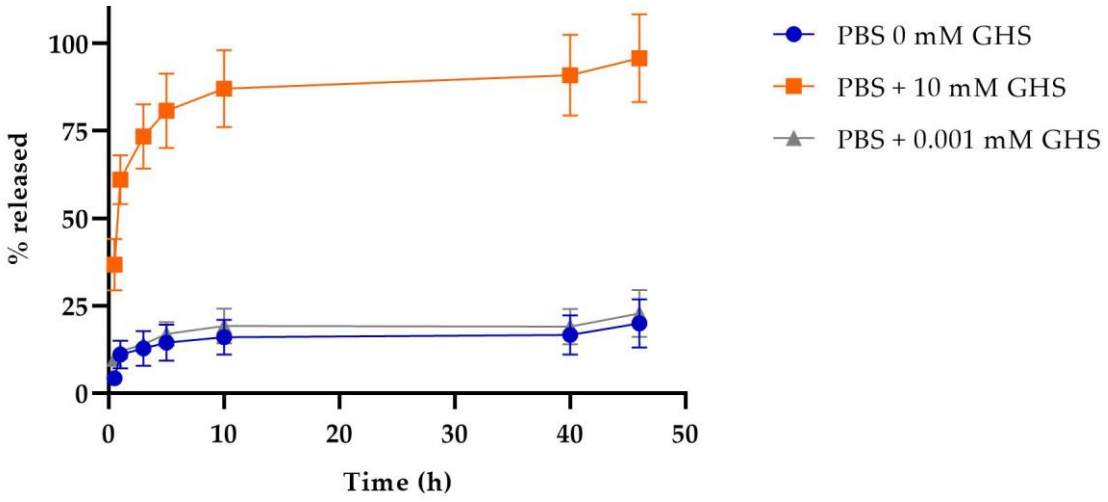

(**a**)

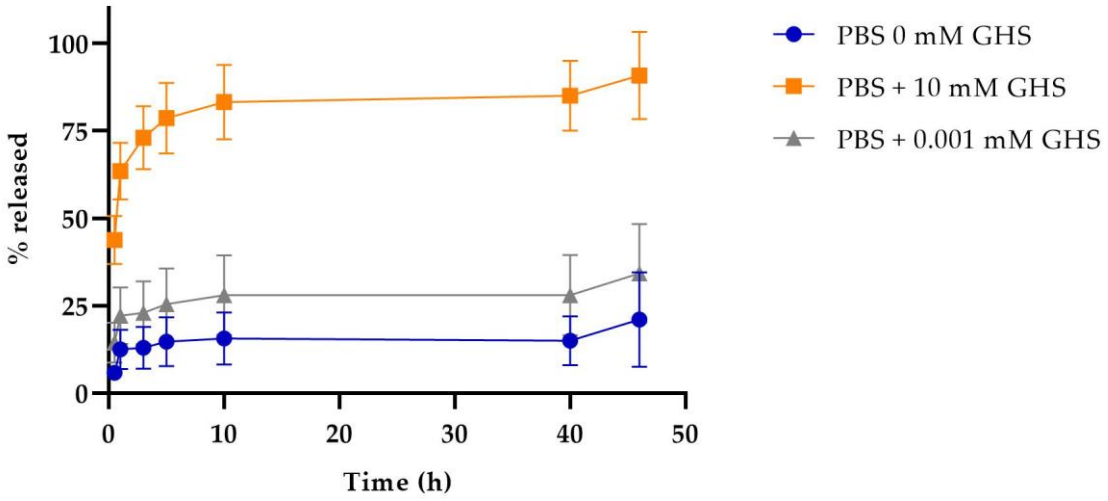

(**b**)

Figure 7. Cytochrome c release profile of nanoparticles under reducing (intracellular) and non-reducing (extracellular) conditions. Cyt c release profile for **a)** NP-253, top and **b)** NP-354, bottom. The data are the averages of three release experiments and the error bars the calculated standard deviations.

2.6. Cell viability and target-specificity studies

To test the effectiveness of the NP-free versus NP-containing system in lung carcinoma cell viability, LLC cells were incubated with either the NP-free formulation (Cyt c-PEG-FA) (**Figure 8a**) or NP formulation (Cyt c-PLGA-PEG-FA, both NP-253 and NP-354) (**Figure 8b**). The NP-free formulation Cyt c-PEG-FA, reduced LLC cell viability up to 50% in a dose-dependent manner, after 6 h of incubation, with an IC_{50} of 129.5 µg/ml (R^2=0.8386), in comparison to non-treated cells. Neither Cyt c alone nor the polymer PEG-FA had any effect on cell viability, supporting that the covalent attachment of PEG-FA to Cyt c allowed Cyt c to induce apoptosis in LLC cells (**Figure 8a**).

The NP formulations, NP-253 and NP-354, both decreased LLC cell viability in a dose-dependent manner (**Figure 8b**). The NP-253 had an IC_{50} at a concentration of 49.2 µg/ml (R^2=0.9781), which showed to be more efficient decreasing cell viability than NP-354 with an IC_{50} =70.1 µg/ml (R^2=0.9781). Therefore, NP-253 and NP-354 formulations showed to be 2.6 and 1.8 times more cytotoxic than the

Peer-reviewed version available at Cancers 2020, 12, 1215; doi:10.3390/cancers12051215

NP-free formulation, which is also a system that can significantly decrease cell viability, but less effectively. Because of its improved performance after 6 h of treatment in LLC cells, we tested the effect of NP-253 after 12 h. However, there was no further improvement in the outcome (**Figure 8c**). These results confirm that the NP-formulation can successfully deliver inside the cells functional Cyt c proteins with an intact structure and activity.

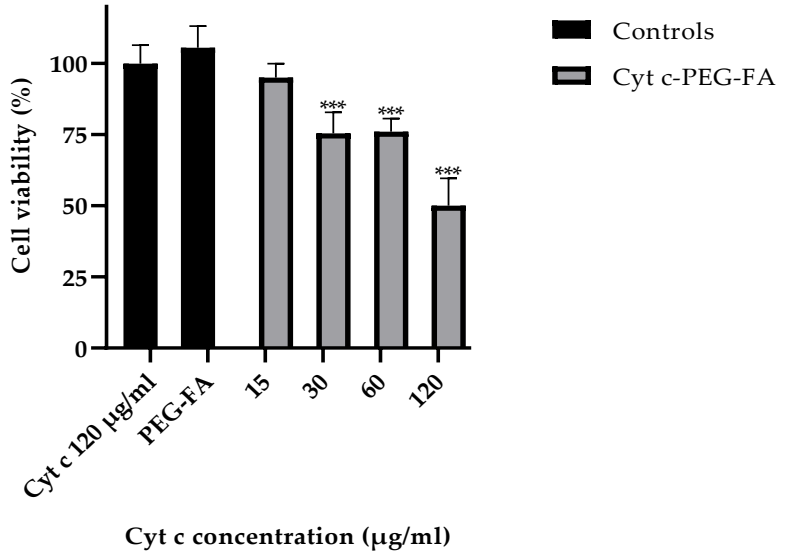

(a)

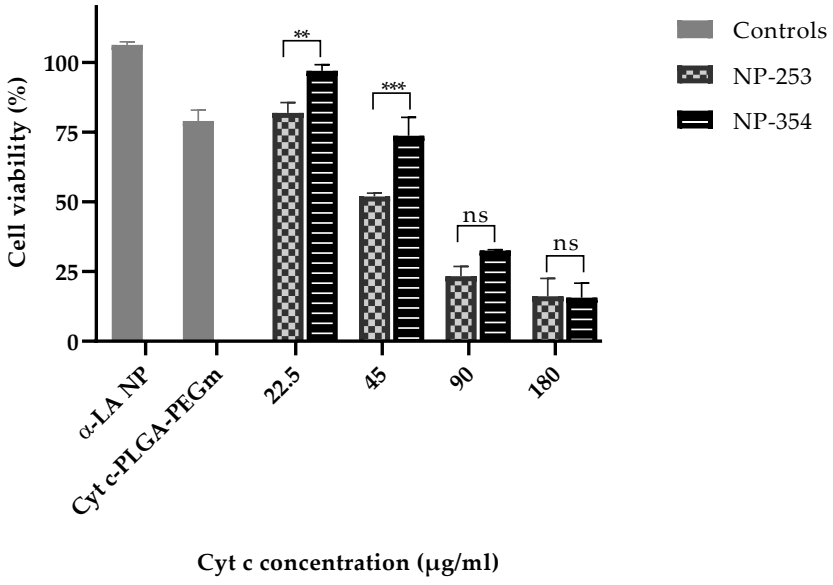

(b)

Peer-reviewed version available at Cancers 2020, 12, 1215; doi:10.3390/cancers12051215

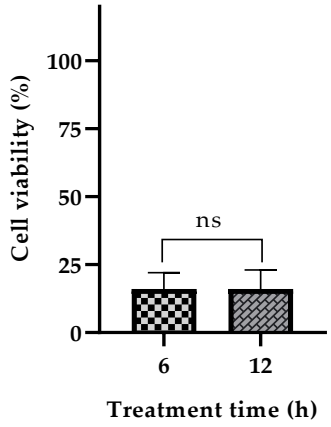

(c)

Figure 8. Cytochrome c delivery in targeted NPs efficiently reduces LLC cell viability after 6 h in a concentration-dependent manner. (a) LLC cell viability assay (MTS) after 6 h of treatment with Cyt c alone (120 µg/ml) and PEG-FA (120 µg/ml) as controls compared to the NP-free formulation Cyt c-PEG-FA at different concentrations (***$p < 0.001$, n=6). **(b)** LLC viability assay after 6 h of treatment with NPs made with non-apoptotic protein α-Lactalbumin (αLA NP) and Cyt c-PLGA-PEG-m (m=metoxi) as controls, compared to the NP formulations NP-253 and NP-354 (**$p= 0.009$ and ***$p< 0.001$, n=3). **(c)** LLC cell viability assay after 6 h and 12 h of treatment with NP-253 (180 µg/ml). Error bars represent the calculated SD.

Next, we tested the selectivity of our system towards cancer cells. NP-253 reduced the viability of LLC cells and HeLa cells (cervical cancer), both overexpressing FR (**Figure 9**). NIH/3T3 (mouse embryonic fibroblasts) and MRC-5 (human fibroblasts derived from lung tissue) were used as healthy control cells that do not overexpress FR. The viability of NIH/3T3 cells was not affected after incubation with NP-253, and MRC-5 cell viability slightly decreased after incubation with the same NP. Nevertheless, the decrease in cell viability of cancer cells after NP-253 was approximately 4-times larger. These results show that the targeted NP-253 drug delivery system is selective towards FR-expressing cancer cells.

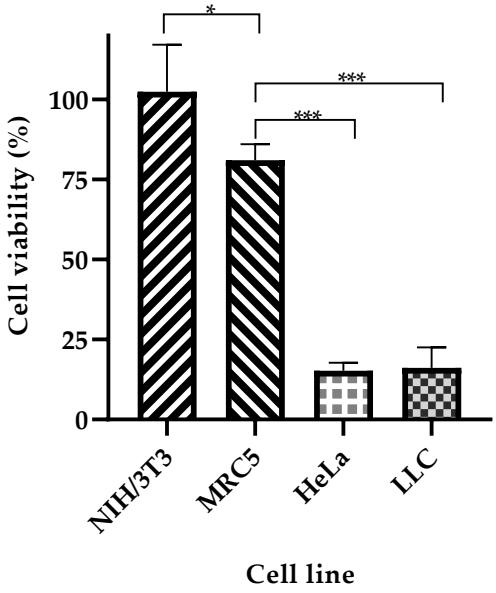

Figure 9. NP-253 decreases the viability of cancerous cell lines compared to non-cancerous cells. Cell viability after treating cancerous (LLC and HeLa cells) and non-cancerous (NIH/3T3 and MRC-

Peer-reviewed version available at Cancers 2020, 12, 1215; doi:10.3390/cancers12051215

5) cells with NP-253 (180 µg/ml of Cyt c) for 6h. One way ANOVA, *p = 0.01 and ***p< 0.001, respectively, n=3. Error bars represent the calculated SD.

2.7. Study of cell death induction using DAPI and propidium iodide co-localization

To confirm if the Cyt c released from NP-253 and NP-354 was structurally functional and induced cell death in LLC, we used a second additional method to MTS, the healthy cell-impermeable and DNA-binding fluorescent stain, propidium iodide (PI). **Figure 10** shows the co-localization of PI in the nucleus of cells treated with both NP-253 and NP-354 formulations, but not in untreated cells. Because PI fluorescence can only be found inside the cells with compromised membranes which are going through a cell-death process, this marker is used to label cells during late apoptosis. These results suggest that cells exposed to the NPs could be decreasing their viability through induction of the apoptotic pathway by Cyt c. This result is also supported by the data showing that the NPs decorating polymers are not toxic to the cells, leaving Cyt c as the only potential cell death inducer.

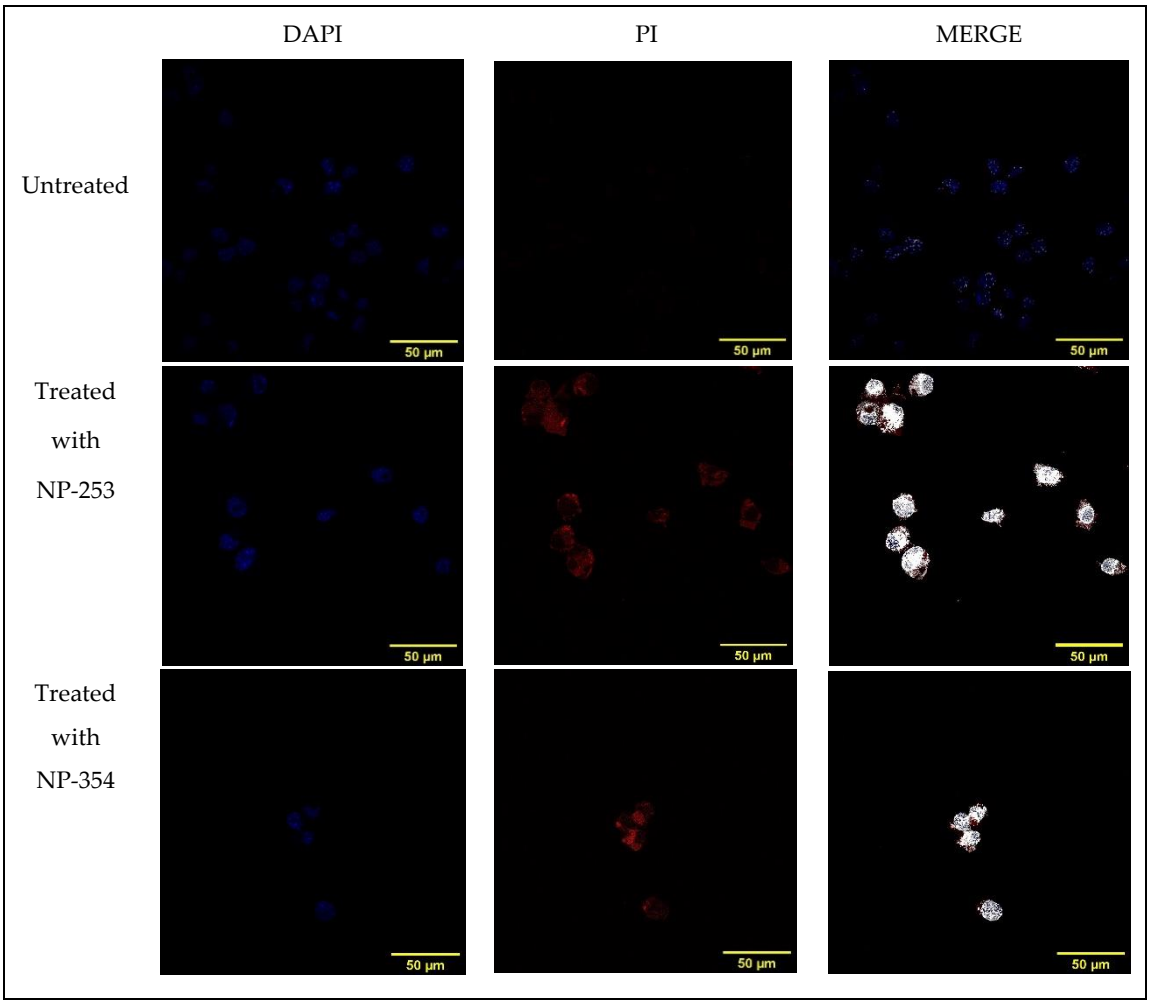

Figure 10. Induction of cell death in LLC cells by NP-253 and NP-354 confirmed by nuclear PI staining. Immunofluorescence of untreated LLC cells (upper panel) shows no co-localization of nuclear DNA dye DAPI (blue) with the cell death (late apoptosis) marker propidium iodide (PI, red), as shown in the upper right panel (merge, white). LLC cells treated 6 h with either NP-253 (middle panel) or NP-354 (lower panel) show co-localization of DAPI and PI (right panels, white color shows co-localization), suggesting compromised membranes and entry of PI inside the nucleus.

2.8. Cyt c-PEG-FA and NP-253 internalization

Peer-reviewed version available at Cancers 2020, 12, 1215; doi:10.3390/cancers12051215

To determine if the FA-containing formulations could be internalized by FR-overexpressing cells, LLC were incubated with FITC-conjugated Cyt c-PEG-FA and NP-253 for 6 h (**Figure 11a**). The presence of the FITC signal within the cytosol is shown by confocal Z-stack images in the Cyt c-PEG-FA-FITC (NP-free control, **Figure 11b**), and the NP-253-FITC (**Figure 11c**), indicating that both formulations were internalized by LLC cells. Nevertheless, the NP formulation showed increased uptake of FA compared to NP-free formulation possibly because it holds more FA-moieties per unit than the NP-free formulation, increasing its probabilities to be endocytosed. These results can be compared to studies performed in different FR-overexpressing cell lines, such as HeLa [23]. Studies show that the binding and uptake of FA attached to other molecules like FITC does not affect the interaction of FA with the FR [23]. Therefore, our NP internalization results are a valid representation and reproduce the kinetics of the folic acid receptor FA-internalization in FR-overexpressing LLC cells.

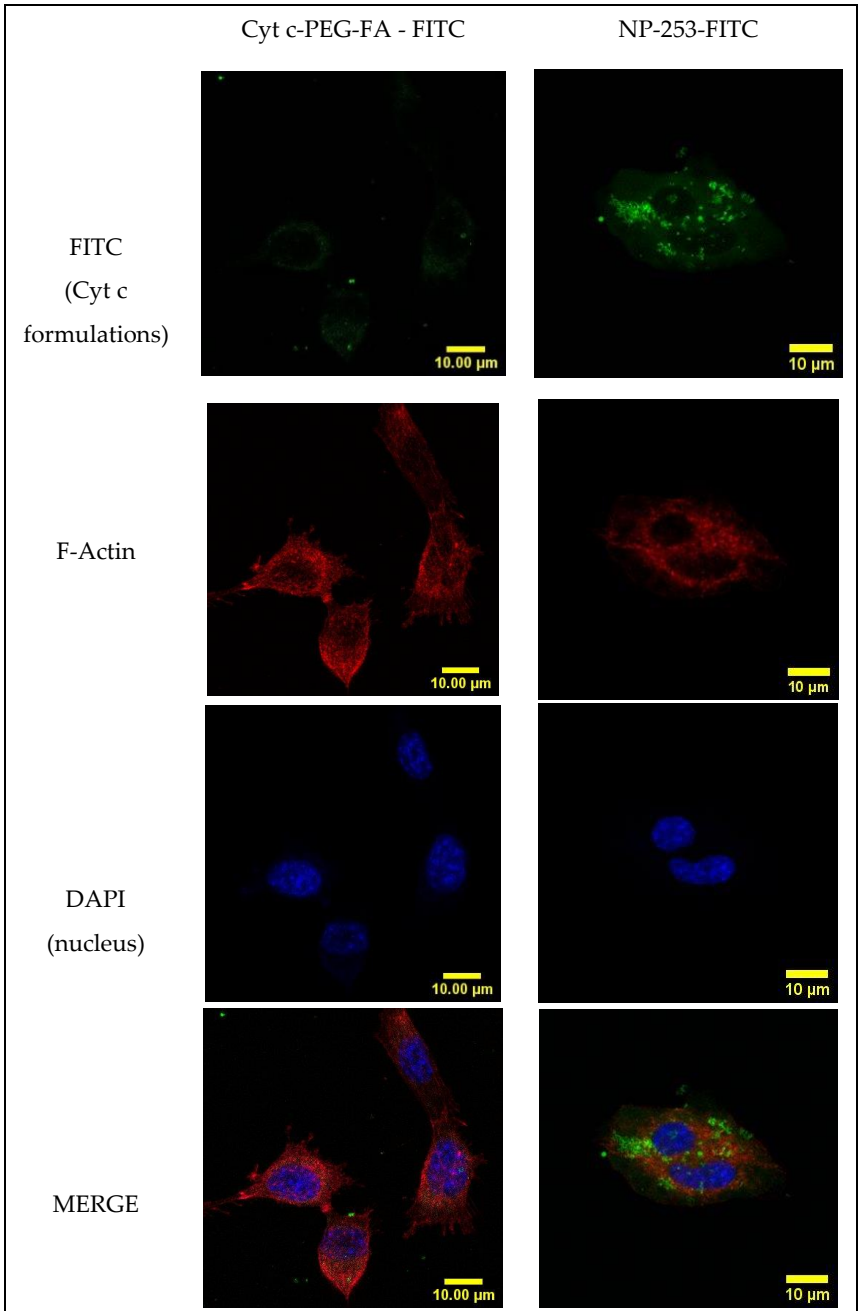

Peer-reviewed version available at Cancers 2020, 12, 1215; doi:10.3390/cancers12051215

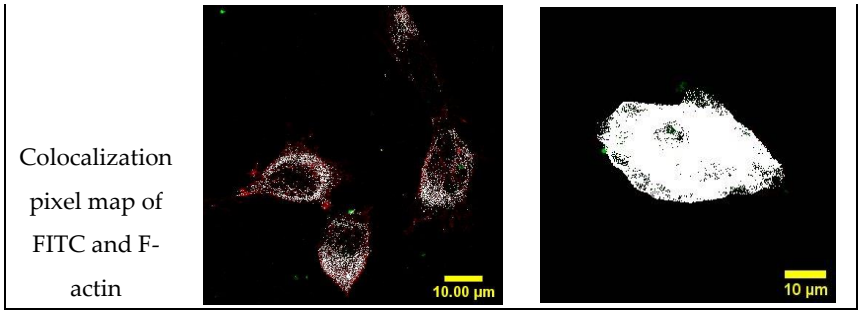

(a)

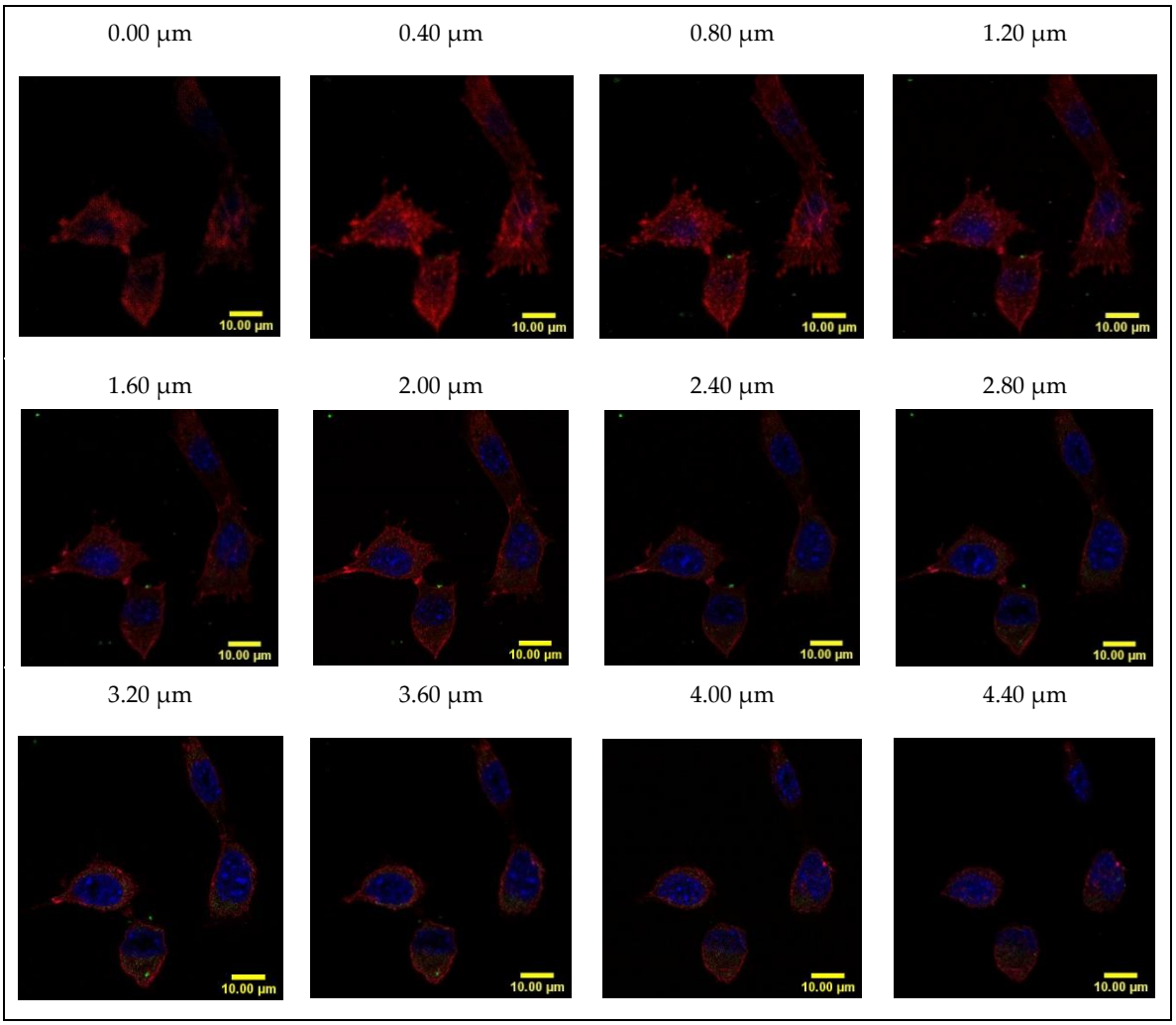

(b)

Peer-reviewed version available at Cancers 2020, 12, 1215; doi:10.3390/cancers12051215

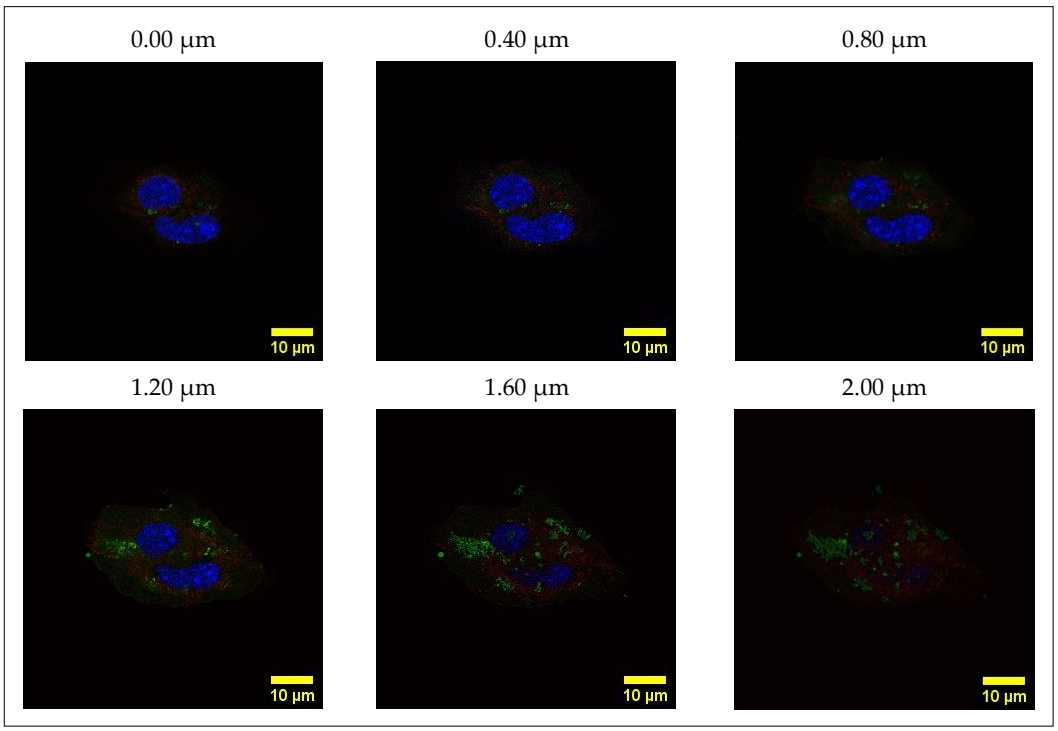

(c)

Figure 11. Internalization of FITC-labeled NP-253 and Cyt c-PEG-FA by LLC cells. (a) Confocal images of LLC cells treated with FITC-labeled Cyt c-PEG-FA and NP-253 (green) after a 6 h incubation. The images shown in the lower panel are the co-localized pixels of FITC (green) and F-actin (red), which are shown in white. Nuclear stain DAPI is shown in blue. **(b)** Consecutive Z-stack images (cell bottom to top) of FITC-labeled Cyt c-PEG-FA (100 µg/ml) treated LLC cells. **(c)** Consecutive Z-stack images (cell bottom to top) of FITC-labeled NP-253 (35 µg/ml) treated LLC cells.

2.9. In-vivo imaging studies of NP biodistribution in a lung carcinoma mouse model

To assess if the NPs target lung tumor *in vivo*, the syngeneic mouse model Lewis Lung Carcinoma was used. In this model, a tumor was induced in C56BL6J mice by injecting subcutaneously (s.c.) Lewis Lung carcinoma cells on the mouse upper back (**Figure 12a, b**). After an average of 10 days of tumor growth, an intravenous injection (tail vein) of infrared (IR)-labeled NP-253 was administered to mice. After injection of IR-NP-253, mice were euthanized at different time points, and organs were extracted to detect if the NPs reached the tumor area/organs, and at which time point (**Figure 13**). After scanning on an infrared detector, a comparison in signal intensity between the control and NP-injected mice (expressed in % observed IR signal of NP-injected mice over control) showed that signal in tumor decreases as time in circulation increases: 5 min: 190%; 1 h: 7%; and 6 h: 8% IR signal. This NP distribution is indicative of compound processing and clearing throughout time (**Figure 13a-c**). Like typical drugs entering through the vessel network, IR NP-293 distributed through the heart, lungs, systemic circulation, and the targeted tumor site. Intravenous administration is one of the best ways for the NPs to be delivered because this route avoids the first-pass effect through the gastrointestinal tract and liver, where many drugs can bind and loose their effective dose before reaching general circulation and their target [26].

Peer-reviewed version available at Cancers 2020, 12, 1215; doi:10.3390/cancers12051215

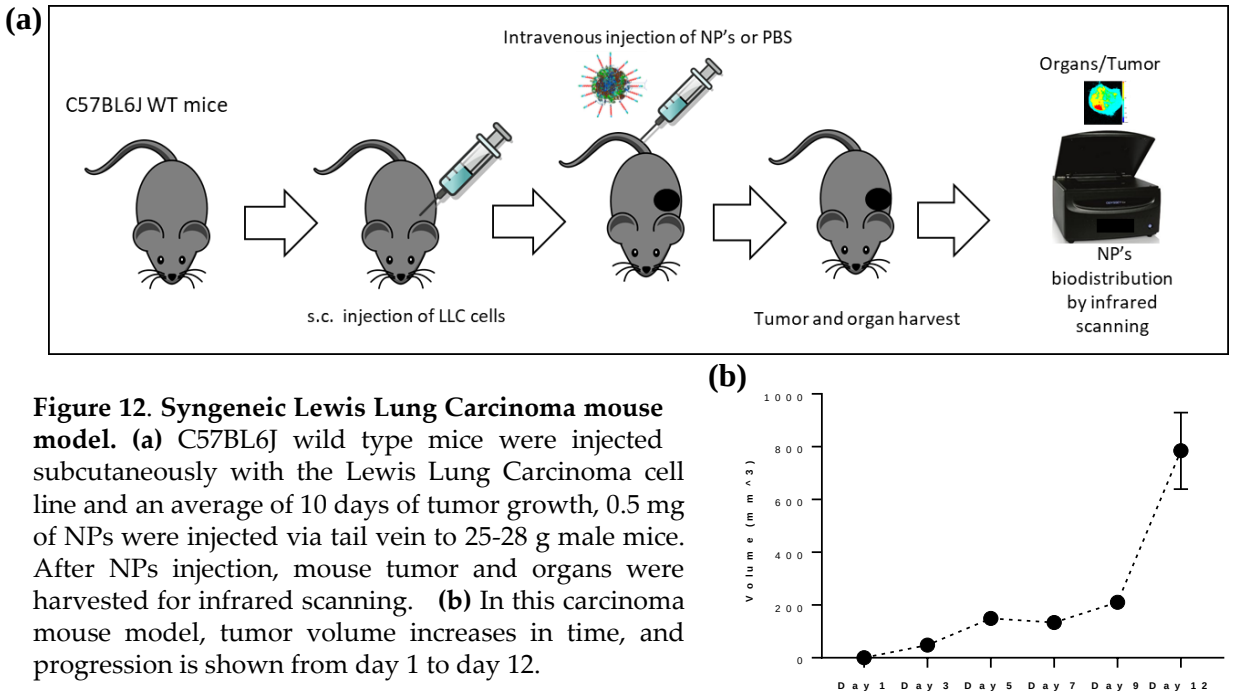

Figure 12. Syngeneic Lewis Lung Carcinoma mouse model. (a) C57BL6J wild type mice were injected subcutaneously with the Lewis Lung Carcinoma cell line and an average of 10 days of tumor growth, 0.5 mg of NPs were injected via tail vein to 25-28 g male mice. After NPs injection, mouse tumor and organs were harvested for infrared scanning. **(b)** In this carcinoma mouse model, tumor volume increases in time, and progression is shown from day 1 to day 12.

The IR-labeled NP-253 solubility was not as high as the unlabeled NP's and their solubility had to be enhanced by adding the excipient trehalose. The upper right panel in **Figure 13a**, showing the red 700 nm channel only, demonstrates how the IR-NP-293 were not degraded or accumulated in a specific organ, but they circulated, reached the tumor site, and continued their path through different organs in the measured time. The infrared signal was obtained by using the infrared pixel quantification scanner and software (Odyssey CLx, Image Studio ™ software). This signal was observed in different mouse tissues at three different time points. At 5 min (**Figure 13a**), we could trace how the i.v.-delivered IR-NP-293 traveled from the vessel network to the pulmonary circulation (5 min: 5117%; 1 h: 202%; 6 h: 0%, IR signal over control in lung tissue). After 1 h (**Figure 13b**), lungs, heart, liver, and spleen retained the largest amount of IR signal, which could indicate that the NPs circulating which did not bind to FR, start to metabolize at this time point. At 6 h after NP injection (**Figure 13c),** kidney, spleen, liver, and brain still showed low IR intensity, and this could be a point where the NPs are at the end of their metabolic processing.

Preprints (www.preprints.org) | NOT PEER-REVIEWED | Posted: 14 April 2020 doi:10.20944/preprints202004.0221.v1

Peer-reviewed version available at Cancers 2020, 12, 1215; doi:10.3390/cancers12051215

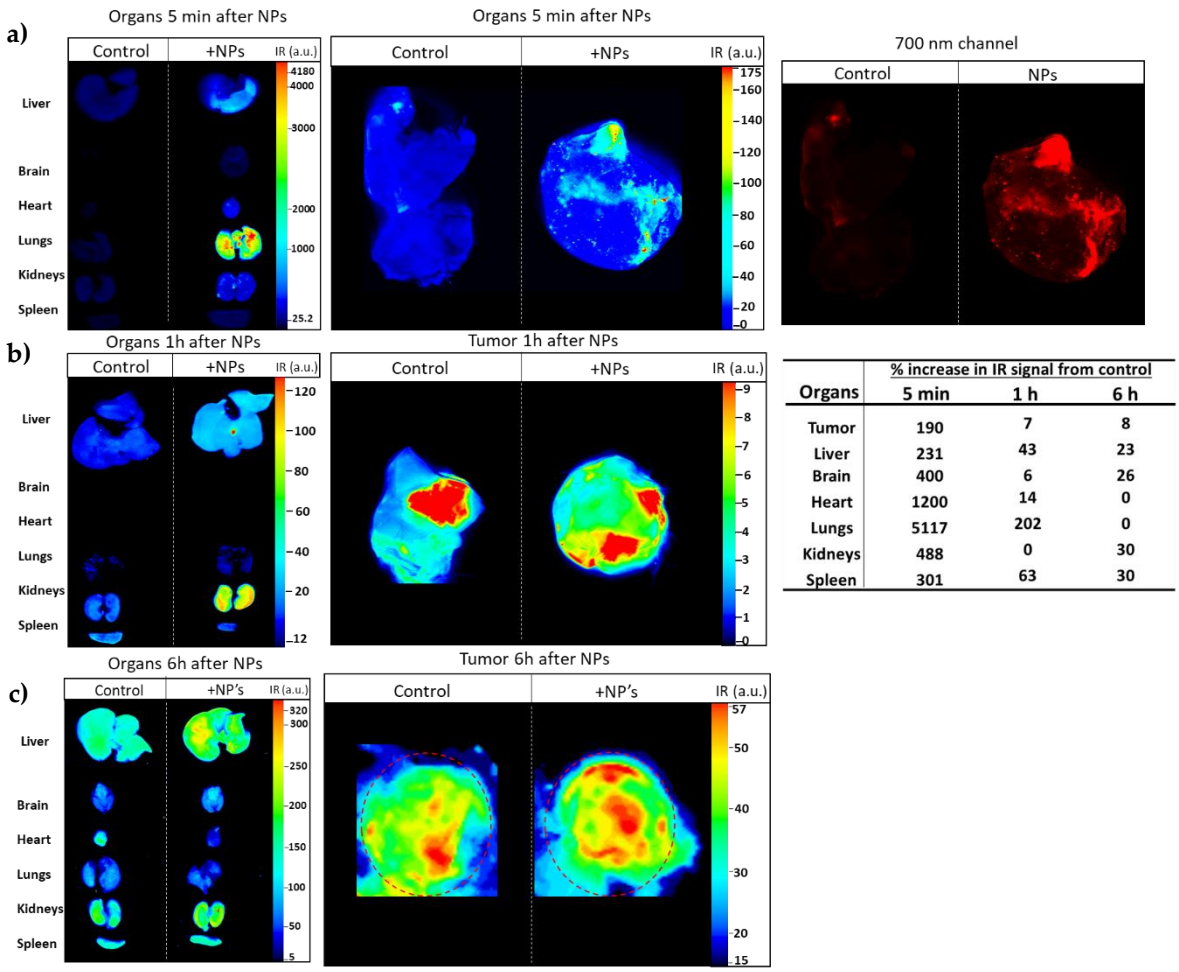

Organs	% increase in IR signal from control		
	5 min	1 h	6 h
Tumor	190	7	8
Liver	231	43	23
Brain	400	6	26
Heart	1200	14	0
Lungs	5117	202	0
Kidneys	488	0	30
Spleen	301	63	30

Figure 13. The IR-labeled NP-253 reaches the tumor area in a Lewis Lung Carcinoma mouse model. (a) Upper panel left and middle images show in multicolor the 700 nm signal intensity (heat map of IR signal intensity areas), representing NP-253 distribution in mouse tumor and organs at 5 min after intravenous (i.v.) injection of NP or control PBS (also having IR background signal). The far-right panel shows the infrared signal from the NPs in the tumor 5 min after i.v. injection only with the red channel (for clarity of NPs distribution in tumor). **(b, c)** Middle and lower panels show a heat map of the IR signal from the NPs or PBS control in the tumor 1 h and 6 h (respectively). The table on the right shows the percent of IR signal (IR pixels) from the tissues of NP-injected mice over the control mice. Each image represents one mouse, n=6.

3. Discussion

In this work, a new method for stabilizing Cytochrome c nanoparticles by covalently coating them with the hydrophobic polymer poly (lactic-co-glycolic) acid (PLGA) was tested. PLGA is a biocompatible, biodegradable, and non-toxic polymer, that has been intensely studied in the field of DDS and has received FDA approval for various applications including drug delivery [27-29]. The idea tested in our studies was to coat the Cyt c NPs with PLGA using a hetero-bifunctional linker, such as succinimidyl 3-(2-pyridyldithio) propionate (SPDP), which includes a disulfide bond, to be able to shed the polymer shell inside the reducing environment of the cell. The presented experiments demonstrated that the tested strategy of folate receptor targeting using a core-shell NP loaded with pro-apoptotic protein Cyt c is an efficient method to deliver this drug and induce cell death in lung carcinoma cells. Both in cell culture and a live lung carcinoma mouse model with an intact immune system, the designed nanoparticles were delivered inside the LLC cells and reached the targeted tumor site after 5 min. The biodistribution of NP-253 after an intravenous application was detected by infrared-labeling in a time-dependent manner at 1 h and 6 h post intravenous administration. The optimized NP's were able to reduce lung carcinoma cell viability in the LLC murine model and in the

human FR overexpressing cervical cancer cells HeLa, three times more than in the non-cancerous cell lines MRC-5 or NIH/3T3 cells, demonstrating cancer-cell target specificity.

Once introduced to a physiological environment, NPs are exposed to adsorption of biomolecules which result in the development of a layer known as the protein corona, which changes the original properties of the nanoparticle. In our system, the formation of this protein corona on the NP surface was regulated by modifying the nanoparticle's surface with the amphiphilic co-polymer folate-poly(ethylene glycol)-poly (lactic-co-glycolic acid)-thiol (FA-PEG-PLGA-SH). Modifications with such polymers have been shown to enhance the colloidal stability and extend the circulation time in blood by enabling the NP to escape from immune system clearance [30,31]. This was the case for our NPs which lasted in circulation in the tumor for at least 6 h after i.v. injection, according to infrared detection.

What about the metabolism of these NPs? The expected metabolites from the nanoparticles include compounds such as PEG, PLGA, Cyt c, and FA. After cellular internalization, PEG is endocytosed and from the early endosome, PEG molecules can be recycled back to the plasma membrane to return to the circulation and finally undergo excretion by the kidney through the urine [30]. PLGA is a biodegradable polymer that is hydrolyzed into lactic acid and glycolic acid, used within the cell [32]; Cyt c will undergo protein catabolism inside cells and reduced to aminoacids; and FA, is a common vitamin that cells uptake and metabolize to produce purines [33]. Thus, we expect little or no toxic secondary effects after repeated intravenous injection of the NPs in mice.

Several studies using folate receptor targeting have employed NIH/3T3 and MRC-5 as control, non-cancerous cell lines that express low folic acid receptor levels [34,35].

In these studies, we demonstrated the target preference of these NPs to folic acid receptor-overexpressing cancer cell lines LLC and HeLa, over MRC-5 and NIH 3T3 cells. Our experiments using HeLa and MRC-5, also show the translational application of our NP formulation to human FR-overexpressing cancer. Uptake of NPs in cancerous murine and human cells, together with the *in vivo* results of tumor-targeting, show that our NPs have cancer cell specificity and tumor-targeting capability. Studies of these NP's and their effect on tumor growth are currently ongoing. We expect the NP-253 to be more effective than NP-354 as its smaller size may allow maximal biological function. Some studies have shown, when comparing different-sized NP's (50 nm, 100 nm and 200 nm NP's), that the smaller NPs had increased tumor penetration, uptake by tumor cells and slowest tumor clearance, leading to a longer retention period in tumor tissue over time and a better efficacy within the tumor microenvironment [36]. Nevertheless, one of the limitations of NP drug delivery systems is conveying the effective dose to induce cell death *in vivo*, and in that aspect, a larger nanoparticle such as the NP-354 or delivery of a more potent drug could have an advantage. Other aspects to take into consideration besides size and drug load is NP surface charge and optimal NP delivery method (tumor-direct or systemic tumor application) which will depend on the type and progress of the targeted tumor [24,37].

After chemical modification of Cyt c to the Cyt c-PEG-FA, NP-free formulation, there was a reduction in the relative caspase activity to 44%, using cell-free caspase 3, 7, and 10 activity assays, compared to the native Cyt c. The reduction of Cyt c activity after crosslinking to the amine groups has been previously reported by our group and is associated with changes in the protein's tertiary structure [23]. The lower activity of Cyt c-PEG-FA can also be due to possible random modifications to the amine groups corresponding to Lys 7, 25, 39 and 72, which play an important role in the interaction of Cyt c with the Apoptotic protease activating factor 1 (Apaf 1) and therefore, in caspase activation [38–40]. On the other hand, the chemical modification of the Cyt c NP surface did not significantly affect the residual activity of Cyt c, retaining 88-96% of its caspase activity. This effect could be attributed to a surface-protein modification only, while most of the Cyt c remained intact in the core of the NP. Thus, Cyt c activity in the Cyt c-PLGA-PEG-FA NP formulation is better preserved than in NP-free formulation Cyt c-PEG-FA.

It has been reported that water nanoprecipitation of Cyt c (10 mg/ml) in the presence of methyl-β-cyclodextrin, using acetonitrile as co-solvent (water:acetonitrile ratio 1:4), followed by surface decoration with the co-polymer PLGA-PEG-FA, results in Cyt c-PLGA-PEG-FA NPs with a diameter of 338 ± 8 nm [12]. We followed a similar methodology for both the polymer and NPs synthesis. The peaks in the SH-PLGA-PEG-FA NMR spectrum are in agreement with the previous reports. To

Peer-reviewed version available at Cancers 2020, 12, 1215; doi:10.3390/cancers12051215

decrease NP size and enhance NP penetration into the tumor, several parameters during the nanoprecipitation procedure were tested, and from all the parameters examined, only alterations in the initial Cyt c concentration led to NP diameter reduction. The correlation of protein concentration with NP diameter, PDI, and precipitation efficiency during nanoprecipitation has shown to be a tendency for other proteins as well [16,41]. Further approaches to reduce Cyt c-PLGA-PEG-FA NPs diameter in our system could be employing a polymer with lower molecular weight.

Cell viability studies showed that NP formulations, specially NP-253, are more cytotoxic than the NP-free formulation Cyt c-PEG-FA, showing a lower IC_{50} (49.2 µg/ml versus 129.5 µg/ml, respectively). This could be attributed to the lower caspase activation residual activity of Cyt c-PEG-FA. The larger loading capacity of Cyt c in the NPs may be adding to the higher toxicity of the formulation. In the case of the NPs, a larger amount of Cyt c can enter the cells with each FR internalized. Fluorescence studies confirmed that both types of formulations (NP-free and NP-containing) are internalized by LLC cells, but the NPs are ~3 times more effective inducing cell death. Studies from our lab have shown that this internalization is mediated by the FR [12,15]. In these studies, it was confirmed that cells treated with the optimized Cyt c-PLGA-PEG-FA NPs were undergoing an apoptotic cell death [42]. One detail we must consider is that we use Cyt c from horse heart, which has approximately 83% identity with human Cyt c [43]. The use of human Cyt c or a more effective/stable recombinant mutant may help broaden the therapeutic potential of this drug delivery system.

In our *in vivo* studies, infrared-labeled NPs (NP-253) followed the classical pattern of intravenously injected drugs, having a peak IR intensity of presence in highly vascularized organs such as lung and heart, brain, tumor, within the first 5 minutes after injection, and decreasing the IR intensity in 1 h, proving that this system can work *in vivo*. Based on the IR intensity of the NP in the organs throughout time, these have already started their metabolism after 1h of circulation in the system, as their signal mostly distributes in kidneys and liver at this time point and continues after 6 h. These NP's were not immediately degraded as they went into the blood, standing undetected and biocompatible in an immune-competent mouse model for at least 6 h. Even though the NP reached places such as the brain, heart, lung, kidneys and liver, the mice showed no sign of toxicity after injection. Long-term exposure studies of mice and pathological analysis of tissues after treatment with NP's are ongoing. Finally, the NPs capability of binding to the tumor, opens way to the development of this NP formulation as a realistic treatment against non-small lung cell carcinoma, following the steps of drugs such as Abraxane ®, a current NP-based, FDA-approved medication to treat lung cancer [28]. Continuing studies are aimed towards the development of a low dose, non-toxic, targeted drug delivery system using the optimized Cyt-c nanoparticle formulation to treat lung carcinoma alone or as adjuvant treatment *in vivo*.

4. Materials and Methods

4.1. Materials

Cytochrome c from equine heart ≥95%, α-Lactalbumin from bovine milk, acetonitrile, ethanol, acetone, dimethylformamide (DMF), reduced glutathione ethyl ester, N,N-diisopropylethylamine (DIEA), tributhylphosphine (PBu3), 3-nitro-2-pyridinesulfenyl chloride (Npys-Cl), Fluoroshield histology mounting medium and fluorescein isothiocyanate isomer I (FITC) were purchased from Sigma-Aldrich (St. Louis, MO). Folate-poly(ethylene glycol)-carboxylic acid FA-PEG-COOH (MW 3,000 Da) and Poly(lactide-co-glycolide)-thiol end cap (Mn: 10,000-30,000 Da) were purchased from Akina, Inc. (West Lafayette, IN). Succinimidyl-3-(2-pyridyldithio) propionate (SPDP) and DAPI (NucBlue®) were obtained from Thermo Fisher Scientific (Waltham, MA). CF™ Dye Phalloidin Conjugates were purchased from Biotium, Inc. (Fremont, CA). D-Trehalose was obtained from Acros Organics. Carboxylic PEG acid, mPEG-COOH (2,000 Da), Folic acid PEG thiol, Folate-PEG-SH (2000 Da) and Folic acid-PEG-FITC (MW 3,400 Da) were purchased from NanoCS (Boston, MA). CellTiter 96 aqueous non-radioactive cell proliferation assay was purchased from Promega Corporation (Madison, WI). CasPASE Apoptosis Colorimetric Assay (caspase 3, 7 and 10) was purchased from G-Biosciences (St. Louis, MO). Near-infrared reactive dye IRDye® 680RD was available as a protein Labeling Kit-High Molecular Weight from LI-COR Biosciences.

Peer-reviewed version available at Cancers 2020, 12, 1215; doi:10.3390/cancers12051215

4.2. Study of the kinetics of folic acid uptake by LLC cells

Lewis Lung carcinoma cells were plated in 24 well plates at a density of 50,000 cells/well and incubated overnight. Cells were incubated with 50µM Folate-PEG-FITC and mPEG-FITC in RPMI medium. After different incubation times, cells were washed with PBS, fixed with 4% paraformaldehyde 20 min at room temperature, and incubated with DAPI (NucBlue®) nuclear stain. In Figure 2, an additional actin stain was added to label the cytoskeleton. After washing three times for 5 min with PBS, fixed cells were mounted in a microscopy slide using fluoroshield mounting media (SIGMA) and analyzed in a confocal microscope (NIKON eclipse) using a 60X objective. The intensity of the images obtained was measured using the program Image J.

4.3. Synthesis of Cyt c-PEG-FA (nanoparticle-free formulation)

Different equivalents of SPDP dissolved in 10 µl of acetonitrile were added to 1 ml of 2 mg/ml Cyt c in PBS-EDTA. The solution was stirred at room temperature for 30 min. The unreacted SPDP was extracted using 10 KDa Amicon Ultra filters. The resulting Cyt c-SDPD was reacted with SH-PEG-FA overnight. The unreacted SH-PEG-FA was separated using 10 KDa Amicon Ultra filters. The product Cyt c-PEG-FA was generated and stored in aliquots at -80^{0}C.

4.4. Protein nanoprecipitation

Cyt c NPs were obtained using a solvent displacement method. Cyt c was dissolved in DI water, at a concentration of 2.5, 5 and 10 mg/ml. Subsequently, the anti-solvent acetonitrile was added at a constant rate of 120 ml/h using an automated syringe pump while stirring constantly at room temperature, keeping a ratio of at least 1:4 water:acetonitrile.

4.5. Determination of precipitation efficiency

After nanoprecipitation, the Cyt c NPs suspension was centrifuged for 10 min at 6.2 x g at room temperature. The supernatant was discharged, and the pellet was lyophilized. The dry NPs were then resuspended in PBS 10 mM pH 7.4, and the concentration was determined by measuring the absorbance at 530 nm and 410 nm using a multimode microplate reader.

4.6. Synthesis of SH-PLGA-PEG-FA

The thiol group in SH-PLGA (MW) was protected with NPys-Cl in anhydrous DMF at RT using 3.3 mg of NPyc-Cl per each 500 mg of SH-PLGA. The product (Nyps-PLGA) was dialyzed against DI water and lyophilized. PLGA-Nyps (400 mg) were mixed with 120 mg of COOH-PEG-FA in anhydrous DMF in the presence of an excess of DIEA. The reaction was stirred overnight under an argon atmosphere. The product (Nyps-PLGA-PEG-FA) was dialyzed against DI water and lyophilized. The Nyps-PLGA-PEG-FA thiol group was deprotected using an excess of PBu_3 in a reaction left overnight at RT in anhydrous DMF and an argon atmosphere. The final product, SH-PLGA-PEG-FA, was dialyzed against DI water and lyophilized.

4.7. ^{1}H NMR

^{1}H NMR spectra of SH-PLGA-PEG-FA co-polymer was acquired with a Bruker 700 FTNMR spectrometer. Spectra were obtained on DMSO-d^6 solutions in 5 mm diameters tubes and chemical shifts are quoted in parts per million relatives to the residual signal of DMSO (δH = 2.50 ppm). The spectra were processed using the Mestrenova (Mnova 11.0 Mestrelab Research) software.

4.8. Synthesis of Cyt c-PLGA-PEG-FA nanoparticles

After nanoprecipitation, the crosslinker SPDP was added to the Cyt c NPs suspension and stirred for 30 min at room temperature. A 1:8 Cyt c-to-linker molar ratio was used. Then the co-polymer SH-PLGA-PEG-FA was dissolved in added acetonitrile. The reaction was stirred overnight at room temperature. Cyt c-PLGA-PEG-FA NPs were centrifuged 10 min 6.2 x g at room temperature and washed three times with DI water.

Peer-reviewed version available at Cancers 2020, 12, 1215; doi:10.3390/cancers12051215

4.9. Dynamic Light Scattering

To determine the diameter and PDI of Cyt c and Cyt c-PLGA-PEG-FA NPs, these were resuspended in acetonitrile and water, respectively. For zeta potential determination Cyt c-PLGA-PEG-FA NPs were resuspended in water and transferred to folded capillary cells. Diameter, PDI and zeta potential were obtained using a zetasizer nano from Malvern (Westborough, MA).

4.10. Scanning electron microscopy

Lyophilized NPs were coated with gold for 50 seconds (10 nm) using a Pepco SC-7 auto sputter coater. Images of coated samples were obtained using a scanning electron microscope at 20 kv.

4.11. Determination of encapsulation efficiency and actual loading

After the overnight reaction for Cyt c-PLGA-PEG-FA NPs synthesis, NPs were centrifuged for 10 min, RT at 6.2 x g. The NPs were washed by resuspending the pellet in DI water and centrifuging three times. NPs were lyophilized and the total yield (mg of dry Cyt c-PLGA-PEG-FA NPs obtained) was determined. The concentration of Cyt c in the supernatants was determined by measuring the absorbance at 530 and 410 nm using a multimode microplate reader. Encapsulation efficiency (EE) and actual loading (AL) were calculated using the following equations:

$$\text{EE: } \frac{Initial\ amount\ of\ Cyt\ c - Cyt\ c\ in\ supernatant}{Initial\ amount\ of\ Cyt\ c} x10, \quad (1)$$

$$AL = \frac{mg\ of\ Cyt\ c\ in\ nanoparticles}{mg\ of\ nanoparticles}\ x\ 100. \quad (2)$$

4.12. Study of the release profile of Cyt c-PLGA-PEG-FA NPs

Both NPs formulation, NP-253 and NP-354, were resuspended at a concentration of 0.5 mg/ml in PBS buffer containing different amounts of GHS (0, 0.001, and 10 mM). Resuspended NPs were incubated at 37^{0}C for a different amount of times: 0.5 h, 1 h, 3 h, 5 h, 10 h, 20 h, and 46 h. After each time point, the suspension was collected and centrifuged for 10 min at 13.8 x g. The supernatants were separated from the pellet to determine the Cyt c concentration released in the supernatant. The pellet was resuspended in the respective buffer and returned to incubation. The Cyt c concentration in the supernatant was determined through UV-vis spectroscopy using a Synergy™ multi-plate reader. The presence of a reducing agent like GHS produces a shift in Cyt c's absorbance peak within the visible region of the spectrum. Therefore, UV-vis scans were performed to measure Cyt c absorbance for each condition and a calibration curve was constructed for each of the release conditions tested. The possible presence of folic acid in the supernatant (which absorbs ~410 nm) from the NP's was considered, and the maximum absorbance where no interference of FA could be detected was used. Thus, the wavelength used to calculate the release of non-reduced Cyt c when incubated in PBS with 0 and 0.001 mM GHS, was 530 nm; while the wavelength to calculate the release of reduced Cyt c incubated in PBS containing 10 mM GHS was at 550 nm. This experiment was performed in triplicate and the results were used to calculate a cumulative release profile curve.

4.13. Cell-free caspase 3, 7 and 10 assay

Cell lysate, samples, and assay were prepared following the protocol of the CasPASE Apoptosis Colorimetric Assay (caspase 3, 7 and 10) from G-Biosciences (St. Louis, MO). Briefly, 5x10^6 HeLa cells were resuspended in 100µl of lysis buffer, flash frozen for 2 min and thawed in a 37˚C bath. After 4 cycles of freezing/thawing of cells, these were centrifuged for 20 min at 4˚C, 11,000 rpm. The supernatant (lysate) was used to continue with the assay. Cell lysate was activated by mixing with a 0.2 mg/ml Cyt c solution in a volume ratio 1:1 and incubation at 37˚C for 150 min. In a 96 well plate, 10 µl of active lysate were mixed with 10 µl of substrate labeled with the chromophore ϱ-nitroanilin (Ac-DEVD-ϱNA) (2mM) and 80 µl of caspase assay buffer. The plate was incubated at 37˚C and the absorbance at 405 nm was monitored periodically.

4.14. In vitro cell viability assay

LLC cells were plated in a 96 well plate at density of 10,000 cells/well. After overnight growth, cells were treated with different Cyt c formulations at different concentrations as well as the respective controls. The MTS (3-(4,5-dimethylthiazol-2-yl)-5-(3-carboxymethoxyphenyl)-2-(4-sulfophenyl)-2H-tetrazolium) cell viability assay from Promega was used and measured in an absorbance plate reader at 490 nm to determine the cell viability after treatment following instructions from the kit manufacturer.

4.15. Calculation of IC_{50} for NP-free Cyt c-PEG-FA formulation and surface-decorated NP-253, NP-354 formulations

To calculate the IC_{50} for the NP-free Cyt c-PEG-FA and the NP formulations NP-253, NP-354, LLC cells were used and an MTS assay was performed following the procedure described above in method *14.4* at the following concentration range for Cyt c-PEG-FA: 15, 30, 60 and 120 µg/ml; and for the NP-253 and NP-354 formulations: 22.5, 45, 90 and 180 µg/ml. The percentiles of viability were transformed using the program Graph Pad Prism to a logarithmic scale using the functions X=Log(X); the Y values were normalized (being 0% the smallest value in the data set and 100% the highest value in the data set); finally a non-linear fit of drug inhibition (log (inhibitor) vs. normalized response-variable slope) was performed to obtain the best fit IC_{50} values, and the R squared. Three experimental replicate results were used for each formulation.

4.16. Study of apoptosis induction using propidium iodide

LLC cells were incubated with 35 µg/ml of Cyt c-PLGA-PEG-FA and after 6 h washed with PBS, and incubated with propidium iodide (PI) for 5 min at 37˚C. Cells were fixed for 20 min at RT using 4% paraformaldehyde and incubated with DAPI (NucBlue®) for 5 minutes. After three washes cells were mounted using fluoroshield mounting media. Untreated cells were subjected to DAPI/PI incubation as well to be used as control.

4.17. Study of formulations for NP internalization

LLC cells were incubated with 35 µg/ml of Cyt c-PLGA-PEG-FA NPs (NP-253) and after 6 h washed with PBS, fixed for 20 min at RT using 4% paraformaldehyde and incubated with DAPI (NucBlue®) for 5 min. After three washes with PBS, cells were mounted using fluoroshield mounting media from Sigma. Untreated cells were used as control. F-Actin of cells were labeled using CF™ Dye Phalloidin Conjugates from Biotium, Inc. (Fremont, CA).

4.18. Cell growth and induction of Lewis Lung Carcinoma in mice

Cell culture of Lewis Lung carcinoma for tumor implant: LLC cells (ATCC CRL-1642) were cultured in High-Glucose Dulbecco's Modified Eagle's Medium (DMEM) supplemented with 10% fetal bovine serum (FBS) and 1% Penicillin/Streptomycin/Amphotericin (PSA) to confluency, and these were gently scraped off the plate, pelleted, quantified. To induce a tumor, mice were subcutaneously injected $1x10^7$ LLC cells in a 400µL total volume composed of 200µL ECM Growth factor reduced gel from Engelbreth-Holm-Swarm murine sarcoma (SIGMA), and 200µL cell suspension in media into the upper right dorsal area of their body.

Mice: Eight-week-old C57BL6J male mice weighing 25-28 g were used. These mice were injected labeled NPs at an average day 10 after tumor implant. Before injection, mice were anesthetized with 1% isoflurane and a tail vein injection of 0.5 mg of labeled NPs with IRDye 680RD was administered in a volume of 200 µL. Mice were euthanized after 5 min, 1 hr or 6 hrs. Tumor and organs were extracted and scanned for NP distribution using the LI-COR Odyssey CLx infrared scanner.

4.19. Labeling of nanoparticles with near infrared dye

To detect NPs in tissue, these were labeled with the near infrared reactive dye IRDye® 680RD (available as a protein Labeling Kit-High Molecular Weight from LI-COR Biosciences). In this reaction

Peer-reviewed version available at Cancers 2020, 12, 1215; doi:10.3390/cancers12051215

an NHS ester (amine-directed) nanoparticle-IRDye crosslink reaction was performed following manufacturer instructions. The steps involving the 680RD dye were performed protecting materials from light. In general, the procedure carried with our NPs was the following: Cyt c-PLGA-PEG-FA nanoparticles used in the in vivo experiments had a diameter of, 253± 55 nm as determined by DLS. These NPs had a composition of 62% of Cyt c and were resuspended in PBS to reach a final Cyt c concentration of 1 mg/ml. NPs were sonicated for 20 min to resuspend. IRDye680 (0.1 mg) was resuspended in ultrapure water to a final concentration of 4 mg/ml. Dye and water were vortexed to ensure full resuspension. Dye prepared was added to Cyt c-PLGA-PEG-FA NPs and these were incubated for two hours at room temperature. After the reaction time - NPs were centrifuged 15 min at 6.2 g x at room temperature. The supernatant was collected, and the pellet resuspended in PBS to wash. A second centrifugation was made for 15 min at 8,000 rpm. The washing step was repeated twice. After the second wash with PBS, the pellets containing the labeled nanoparticles were frozen and lyophilized.

4.20. Nanoparticle optimization for in vivo tumor targeting

To optimize the in vivo targeting of the tumors, NPs were size-reduced, and an excipient was added to improve solubility. To perform co-lyophilization of Cyt c-PLGA-PEG-FA NPs the excipient trehalose, they were first synthesized by nanoprecipitation. After an overnight synthesis reaction, Cyt c-PLGA-PEG-FA NPs were centrifuged for 10 min, speed of 6.2 x g, at RT. The supernatant was discarded, and the pellet resuspended in 1 ml of a trehalose solution (2 mg/ml). The centrifugation and resuspension of the pellet was repeated twice to wash the NPs. After a third centrifugation, NPs were resuspended in 1 ml of trehalose solution containing 1:2 nanoparticles:trehalose weight ratio and lyophilized as a suspension in this solution.

NPs diameter determination: After Cyt c-PLGA-PEG-FA NPs were lyophilized these were resuspended in DI water and sonicated for 5 min. The diameter was determined using Dynamic Light Scattering (DLS) (seta sizer from Malvern). The results are the average of three runs and the Cyt c-PLGA-PEG-FA NP's used in this *in vivo* assay had a diameter of 253 nm.

4.21. Detection of infrared-labeled nanoparticles in vivo

NPs detection in tissues was made using the LI-COR Odyssey CLx near-infrared imaging system. A 169µm resolution and a medium quality setting were chosen in the Image Studio™ imaging software. All the tumor or the organ area was selected for quantification and the IR signal was obtained using the Image Studio™ software. To obtain the percentage of IR signal of the NP-injected mice over the control mice, the following formula was used:

% IR signal of NP-injected tissue over control tissue: $[\frac{IR\ signal\ from\ NP\ injected\ mouse}{IR\ signal\ of\ control\ mouse} x100] - 100$

5. Conclusions

We confirmed the superiority of nano-sized NP formulations over individual Cyt c tagged with FA. Our optimized NP formulation retained 88-96% of Cyt c activity, inducing apoptosis and decreasing lung carcinoma cell viability with a lower IC_{50} than the NP-free formulation. A reduction of around 100 nm (30%) in NP diameter was achieved enhancing the previously reported system which had a diameter of 338 ± 8 nm. The optimized Cyt c PLGA-PEG-FA NPs showed selective cytotoxicity towards non-small cell lung carcinoma cells overexpressing FR including LLC and HeLa, but not towards normal cells. *In-vivo* studies showed that these NPs are biocompatible, immune-system resistant, they can quickly bind to LLC tumors, 5 min after application by intravenous route, and remain in circulation at least 6 h. These results open way to the *in vivo* testing of this NP formulation as a targeted drug delivery system for the treatment of lung carcinoma or other FA-overexpressing tumors.

Author Contributions: conceptualization, V.BB., Y.FA., K.G., and A.M.; methodology, V.BB., Y.FA, and K.G; validation, V.BB., Y. FA., K.G., and A.M; formal analysis, V.BB. and Y.FA; investigation, V.BB., I.DM., F.JO., L.A., E.CR., K.MA., and Y.FA. ; resources, Y.FA., K.G., and A.M.; data curation, V.BB. and Y.FA; writing—original draft preparation, V.BB., Y.FA, and K.G; writing—review and editing, V.BB., Y.F., K.G., A.M., I. DM., F. JO. and L.A.; visualization, V.BB. and Y.FA.; supervision, Y.FA., K.G., A. M., and V.BB.; project administration, Y.FA. and K.G.; funding acquisition, Y.FA. and K.G.

Funding and approvals: Research reported in this publication was funded by the National Institute on Minority Health and Health Disparities (NIMHD) and the National Institute of Allergy and Infectious Diseases (NIAID) of the National Institutes of Health under Award Number U54MD007587. The content is solely the responsibility of the authors and does not necessarily represent the official views of the National Institutes of Health. All necessary approvals from the Institutional Animal Care and Use Committee (IACUC) were in place for the performed research: Assurance ID number: D16-00343, IACUC Protocol Universal Number: 048-2018-15-01.

Acknowledgments: We acknowledge the Biomedical Engineering Department at Florida International University for supplying some of the facilities used for the execution of this research. To the Puerto Rico Science Technology and Research Trust for the Continuity Track grant to continue research projects with collaborators outside the Caribbean region used to buy materials for this research. To the Molecular Science Research Center for support to VBB by granting a fellowship. To Dr. David I Kreiger for his help with the synthesis of PLGA-PEG-FA.

Conflicts of Interest: The authors declare no conflict of interest. The funders had no role in the design of the study; in the collection, analyses, or interpretation of data; in the writing of the manuscript, or in the decision to publish the results.

References

1. Fouad, Y.A.; Aanei, C. Revisiting the hallmarks of cancer. *Am J Cancer Res.* **2017**, *7*, 1016–1036.
2. Lopez, J.; Tait, S.W.G. Mitochondrial apoptosis: killing cancer using the enemy within. *Br. J. Cancer* **2015**, *112*, 957–962.
3. Jaiswal, P. K., Goel, A., & Mittal, R. D. Survivin: A molecular biomarker in cancer. *Indian J. Med. Res.* **2015,** *141*: 389–397.
4. Pandey, M. K.; Prasad, S.; Tyagi, A. K.; Deb, L.; Huang, J.; Karelia D. N.; Amin, S. G. & Aggarwal, B. B. Targeting Cell Survival Proteins for Cancer Cell Death. *Pharmaceuticals (Basel, Switzerland)* **2016,** *9*: 11.
5. Pfeffer, C.; Singh, A. Apoptosis: a target for anticancer therapy. *Int. J. Mol. Sci.* **2018**, *19*, 448.
6. Jiang, X.; Wang, X. Cytochrome C-mediated apoptosis. *Annu. Rev. Biochem.* **2004**, *73*, 87–106.
7. Kumar, R.; Bhat, T.A.; Walsh, E.M.; Chaudhary, A.K.; O'Malley, J.; Rhim, J.S.; Wang, J.; Morrison, C.D.; Attwood, K.; Bshara, W.; et al. Cytochrome c deficiency confers apoptosome and mitochondrial dysfunction in African-American men with prostate cancer. *Cancer Res.* **2019**, *79*, 1353–1368.
8. Srinivasan, S.; Guha, M.; Dong, D.W.; Whelan, K.A.; Ruthel, G.; Uchikado, Y.; Natsugoe, S.; Nakagawa, H.; Avadhani, N.G. Disruption of cytochrome c oxidase function induces the Warburg effect and metabolic reprogramming. *Oncogene* **2016**, *35*, 1585–1595.
9. Li, F.; Srinivasan, A.; Wang, Y.; Armstrong, R.C.; Tomaselli, K.J.; Fritz, L.C. Cell-specific induction of apoptosis by microinjection of cytochrome c. Bcl-xL has activity independent of cytochrome c release. *J. Biol. Chem.* **1997**, *272*, 30299–30305.

10. Zhivotovsky, B.; Orrenius, S.; Brustugun, O.T.; Døskeland, S.O. Injected cytochrome c induces apoptosis. *Nature* **1998**, *391*, 449–450.
11. Santra, S.; Kaittanis, C.; Perez, J.M. Cytochrome c encapsulating theranostic nanoparticles: A novel bifunctional system for targeted delivery of therapeutic membrane-impermeable proteins to tumors and imaging of cancer therapy. *Mol. Pharm.* **2010**, *7*, 1209–1222.
12. Morales-Cruz, M.; Cruz-Montañez, A.; Figueroa, C.M.; González-Robles, T.; Davila, J.; Inyushin, M.; Loza-Rosas, S.A.; Molina, A.M.; Muñoz-Perez, L.; Kucheryavykh, L.Y.; et al. Combining stimulus-triggered release and active targeting strategies improves cytotoxicity of cytochrome c nanoparticles in tumor cells. *Mol. Pharm.* **2016**, *13*, 2844–2854.
13. Figueroa, C.M.; Suarez, B.; Molina, A.; Mendez, J.; Torres, Z.; Griebenow, K. Smart release nano-formulation of cytochrome c and hyaluronic acid induces apoptosis in cancer cells. *J Nanomed. Nanotechnol.* **2017**, *08*.
14. Saxena, M.; Delgado, Y.; Sharma, R.K.; Sharma, S.; Guzmán, S.L.P.D.L.; Tinoco, A.D.; Griebenow, K. Inducing cell death in vitro in cancer cells by targeted delivery of cytochrome c via a transferrin conjugate. *PLoS One* **2018**, *13*, e0195542.
15. Kucheryavykh, Y.V.; Davila, J.; Ortiz-Rivera, J.; Inyushin, M.; Almodovar, L.; Mayol, M.; Morales-Cruz, M.; Cruz-Montañez, A.; Barcelo-Bovea, V.; Griebenow, K.; et al. Targeted delivery of nanoparticulate Cytochrome C into glioma cells through the proton-coupled folate transporter. *Biomolecules* **2019**, *9*, 154.
16. Morales-Cruz, M.; Flores-Fernández, G.M.; Morales-Cruz, M.; Orellano, E.A.; Rodriguez-Martinez, J.A.; Ruiz, M.; Griebenow, K. Two-step nanoprecipitation for the production of protein-loaded PLGA nanospheres. *Res. Pharm. Sci.* **2012**, *2*, 79–85.
17. Morales-Cruz, M.; Figueroa, C.M.; González-Robles, T.; Delgado, Y.; Molina, A.; Méndez, J.; Morales, M.; Griebenow, K. Activation of caspase-dependent apoptosis by intracellular delivery of cytochrome c-based nanoparticles. *J. Nanobiotechnology* **2014**, *12*.
18. Cheng, R.; Feng, F.; Meng, F.; Deng, C.; Feijen, J.; Zhong, Z. Glutathione-responsive nano-vehicles as a promising platform for targeted intracellular drug and gene delivery. *J. Control. Release* **2011**, *152*, 2–12.
19. Fernández, M.; Javaid, F.; Chudasama, V. Advances in targeting the folate receptor in the treatment/imaging of cancers. *Chem. Sci.* **2018**, *9*, 790–810.
20. Grodzinski, P.; Kircher, M.; Goldberg, M.; Gabizon, A. Integrating Nanotechnology into Cancer Care. *ACS Nano* **2019**, *13*, 7370–7376.
21. Kellar, A.; Egan, C.; Morris, D. Preclinical murine models for lung cancer: clinical trial applications. *BioMed Research International* **2015**, *2015*, 1–17.
22. Chhabra, R.; Tosi, G.; Grabrucker, A. Emerging use of nanotechnology in the treatment of neurological disorders. *Curr. Pharm.* **2015**, *21*, 3111–3130.23.
23. Mendez, J.; Morales-Cruz, M.; Delgado, Y.; Figueroa, C.M.; Orellano, E.A.; Morales, M.; Monteagudo, A.; Griebenow, K. Delivery of chemically glycosylated cytochrome c immobilized in mesoporous silica nanoparticles induces apoptosis in HeLa cancer cells. *Mol. Pharm.* **2014**, *11*, 102–111.
24. Rosenblum, D.; Joshi, N.; Tao, W.; Karp, J. M.; Peer, D. Progress and challenges towards targeted delivery of cancer therapeutics. *Nature communications*, **2018,** *9*, 1410.

25. Wu, G.; Fang, Y.-Z.; Yang, S.; Lupton, J.R.; Turner, N.D. Glutathione metabolism and its implications for health. *J. Nutr.* **2004**, *134*, 489–492.
26. Chenthamara, D.; Subramaniam, S.; Ramakrishnan, S. G.; Krishnaswamy, S.; Essa, M. M.; Lin, F. H.; Qoronfleh, M. W. Therapeutic efficacy of nanoparticles and routes of administration. *Biomaterials Res.* **2019**,*23*, 20.
27. Bobo D.; Robinson, K.J.; Islam, J; Thurecht, K.J.; Corrie, S.R. Nanoparticle-Based Medicines: A Review of FDA-Approved Materials and Clinical Trials to Date. *Pharm. Res.* **2016**, *33*,2373–87.
28. Gonda, A.; Zhao, N.; Shah, J. V.; Calvelli, H. R.; Kantamneni, H.; Francis, N. L.; Ganapathy, V. Engineering Tumor-Targeting Nanoparticles as Vehicles for Precision Nanomedicine. *Med. One* **2019**, *4*, e190021.
29. Baumann, A.; Tuerck, D.; Prabhu, S.; Dickmann, L.; Sims, J. Pharmacokinetics, metabolism and distribution of PEGs and PEGylated proteins: quo vadis? *Drug Discov Today*. **2014**, *19*, 1623-31.
30. Kang, B.; Okwieka, P.; Schöttler, S.; Winzen, S.; Langhanki, J.; Mohr, K.; Opatz, T.; Mailänder, V.; Landfester K.; Wurm, F.R. Carbohydrate-Based Nanocarriers Exhibiting Specific Cell Targeting with Minimum Influence from the Protein Corona. *Angew. Chem. Int. Ed. Engl.* **2015**, *54*, 7436-40.
31. Dai, Q.' Walkey, C.; Chan, W. C. Polyethylene glycol backfilling mitigates the negative impact of the protein corona on nanoparticle cell targeting. *Angew. Chem. Int. Ed*., **2014**, *53*, 5093–5096.
32. Makadia, H.K.; Siegel, S.J. Poly Lactic-co-Glycolic Acid (PLGA) as Biodegradable Controlled Drug Delivery Carrier. *Polymers (Basel)* **2011,** *3*,1377-1397.
33. Huennekens, F.M.; Folic acid coenzymes in the biosynthesis of purines and pyrimidines. *Vitam. Horm.* **1968,** *26*, 375-94.
34. Yu, Y.; Wang, J.; Kaul, S. C.; Wadhwa, R.; Miyako, E. Folic Acid Receptor-Mediated Targeting Enhances the Cytotoxicity, Efficacy, and Selectivity of Withania somnifera Leaf Extract: *In vitro* and *in vivo* Evidence. *Front. Oncol.* **2019**, *9*, 602.
35. Elkhodiry, M. A.; Husseini, G. A.; Velluto, D. Targeting the Folate Receptor: Effects of Conjugating Folic Acid to DOX Loaded Polymeric Micelles. *Anti-Cancer Agent Me* **2016,** *16*, 1275–1280.
36. Tang, L., Fan, T. M., Borst, L. B. & Cheng, J. Synthesis and biological response of size-specific, monodisperse drug–silica nanoconjugates. *ACS Nano.* **2012**, *6*, 3954–3966.
37. Morales-Cruz, M., Delgado, Y., Castillo, B., Figueroa, C. M., Molina, A. M., Torres, A., Milián, M., & Griebenow, K. Smart Targeting To Improve Cancer Therapeutics. *Drug des. devel. ther.,* **2019**, *13*, 3753–3772.
38. Kluck, R.M.; Ellerby, L.M.; Ellerby, H.M.; Naiem, S.; Yaffe, M.P.; Margoliash, E.; Bredesen, D.; Mauk, A.G.; Sherman, F.; Newmeyer, D.D. Determinants of cytochrome c pro-apoptotic activity. The role of lysine 72 trimethylation. *J. Biol. Chem.* **2000**, *275*, 16127–16133.
39. Yu, T.; Wang, X.; Purring-Koch, C.; Wei, Y.; McLendon, G.L. A mutational epitope for Cytochrome c binding to the apoptosis protease activation Factor-1. *J Biol Chem.,* **2001**, *276*, 13034–13038.
40. Hao, Z.; Duncan, G.S.; Chang, C.-C.; Elia, A.; Fang, M.; Wakeham, A.; Okada, H.; Calzascia, T.; Jang, Y.; You-Ten, A.; Yeh, W. C.; Ohashi, P.; Wang, X.; Mak, T. W. Specific ablation of the apoptotic functions of Cytochrome c reveals a differential requirement for Cytochrome c and Apaf-1 in apoptosis. *Cell,* **2005**, *121*, 579–591.

41. Langer, K.; Balthasar, S.; Vogel, V.; Dinauer, N.; von Briesen, H.; Schubert, D. Optimization of the preparation process for human serum albumin (HSA) nanoparticles. *Int. J. Pharm.* **2003**, *257*, 169–180.
42. Santucci, R.; Sinibaldi, F.; Cozza, P.; Polticelli, F.; Fiorucci, L. Cytochrome c: An extreme multifunctional protein with a key role in cell fate. *Int. J. Biol. Macromol.* **2019**, *136*, 1237–1246.
43. Kulkarni, K.; Sundarrajan, P. A Study of Phylogenetic Relationships and Homology of Cytochrome C using Bioinformatics. *Int. Res. J. of Sci. Eng.* **2016**, *4*, 11.